Sedimentary Geology 383 (2019) 101–120

Contents lists available at ScienceDirect

Sedimentary Geology

journal homepage: www.elsevier.com/locate/sedgeo

Organic matter content and type variation in the sequence stratigraphic context of the Upper Devonian New Albany Shale, Illinois Basin

Bei Liu [a,*], Juergen Schieber [a], Maria Mastalerz [b], Juan Teng [b,c]

[a] Department of Earth and Atmospheric Sciences, Indiana University, Bloomington, IN 47405, USA
[b] Indiana Geological and Water Survey, Indiana University, Bloomington, IN 47405-2208, USA
[c] Department of Petroleum Engineering, Chengdu University of Technology, Chengdu, Sichuan 610059, China

ARTICLE INFO

Article history:
Received 4 December 2018
Received in revised form 7 February 2019
Accepted 8 February 2019
Available online 14 February 2019

Editor: Dr. J. Knight

Keywords:
Organic matter
Devonian black shales
Sequence stratigraphy
Paleoproductivity
Clastic supply
Bottom-water redox condition

ABSTRACT

Organic matter quantity and type are important parameters in conventional source rock evaluation and unconventional shale oil/gas reservoir characterization. Understanding the stratigraphic distribution of organic matter content and type in black shale successions is critical for identifying potentially productive intervals, because organic matter can adsorb large amounts of oil and gas. Detailed examination of total organic carbon content, organic petrographic composition, and high-resolution (8 cm spacing) geochemical proxies in a sequence stratigraphic framework were conducted on an early mature (0.55% R_o) New Albany Shale core of the Illinois Basin to study the influence of relative sea-level fluctuations on paleoproductivity, clastic supply, bottom-water redox conditions, and their combined control on total organic carbon distribution pattern and organic maceral variation.

Marine organic matter including amorphous organic matter and alginite (mainly derived from *Tasmanites* cysts) is the dominant organic matter in the New Albany Shale. Terrestrial organic matter accounts for <10% of total organic matter. Within a sequence stratigraphic context, total organic carbon content increases in transgressive systems tracts, reaches a maximum before the maximum flooding surface, and shows relatively low values in highstand systems tracts. Comparatively, low total organic carbon contents at maximum flooding surfaces reflect a combination of low sedimentation rates, elevated bottom-water oxygenation, and high biogenic silica dilution. Stratigraphically, amorphous organic matter content increases in transgressive systems tracts, reaches a maximum near the maximum flooding surface, and decreases in highstand systems tracts. Enrichment of broken *Tasmanites* cysts and their detrital infills are an indicator of high-energy environments and could possibly indicate lowstand systems tracts. The stratigraphic distribution of organic matter content and type may result in cyclic stratigraphic variations of hydrocarbon generation potential and oil saturation, and influence the development of secondary organic pores when the New Albany Shale is within the oil and gas windows.

1. Introduction

Organic matter (OM) richness, type, and thermal maturity are key parameters used in the evaluation of conventional and unconventional petroleum systems (Tissot and Welte, 1984; Peters and Cassa, 1994; Jarvie, 2012a, 2012b; Hackley and Cardott, 2016). The total organic carbon (TOC) content in source rocks determines the quantity of generated petroleum and the type of kerogen controls the type of generated hydrocarbons (Tissot and Welte, 1984). OM-hosted pores play a significant role in oil and gas storage and migration in unconventional petroleum systems because of their large specific surface area and organic affinity (Passey et al., 2010; Schieber, 2010; Loucks et al., 2012; Liu et al., 2017). However, most organic pores are <1000 nm (Wang et al., 2009; Schieber, 2010; Loucks et al., 2012) and contribute differently in shale oil vs shale gas systems because of the difference in fluid properties of oil vs gas (Jarvie, 2012a, 2012b; Bohacs et al., 2013). OM content in source rocks is not uniformly distributed stratigraphically or spatially (Creaney and Passey, 1993; Slatt and Rodriguez, 2012; Dong et al., 2017), and OM is not homogeneous in composition, but is composed of a mixture of organic macerals (e.g., Robl et al., 1992; Stasiuk and Fowler, 2004; Mastalerz et al., 2012, 2013; Hackley and Cardott, 2016; Liu et al., 2017, 2019; Abarghani et al., 2018; Harris et al., 2018; Ponsaing et al., 2018). Therefore, documenting TOC distribution and organic maceral variation in a sequence stratigraphic context is of great significance for the evaluation of conventional source rocks and unconventional shale oil/gas resources.

Primary controls on OM accumulation in marine sediments include paleoproductivity, preservation conditions (bottom-water redox conditions), clastic supply, as well as sedimentation rate (Sageman et al., 2003; Rimmer et al., 2004; Bohacs et al., 2005, 2013). Sedimentation rate can affect preservation conditions of OM and tie accumulation of organic-rich mudstones to a sequence stratigraphic framework

* Corresponding author.
E-mail address: liubei@iu.edu (B. Liu).

https://doi.org/10.1016/j.sedgeo.2019.02.004
0037-0738/

(Schwalbach and Bohacs, 1992; Bohacs et al., 2005). Cyclic fluctuations of relative sea level affect accommodation, water depth, and nutrient supply, and influence the parameters that control the deposition of organic-rich sediments (Creaney and Passey, 1993; Sageman et al., 2003; Slatt and Rodriguez, 2012; Dong et al., 2017; Byun et al., 2018). In general, when sea level rises, detrital input and oxygen content in bottom water decrease, and in combination they result in sediment-starved conditions and OM accumulation. In contrast, when sea level drops, increased clastic supply and better oxygenation of bottom water result in enhanced microbial degradation of OM and the deposition of bioturbated organic-poor strata. Previous studies have reported that shales deposited in transgressive systems tracts (TSTs) have been found to be more enriched in OM than shales deposited in highstand systems tracts (HSTs) (Lazar, 2007; Slatt and Rodriguez, 2012; Dong et al., 2017).

OM in petroleum source rocks can be classified into four types of kerogens on the basis of H/C versus O/C ratios (Tissot et al., 1974; Peters and Cassa, 1994). However, examining them with a reflected-light microscope reveals added complexity through the recognition of a variety of organic macerals which have different sources and formation processes (Peters and Cassa, 1994; Taylor et al., 1998). Stratigraphic variation of OM type has been previously studied in black shale successions (Pasley et al., 1991; Gregory and Hart, 1992; Robison et al., 1996; Bialkowski et al., 2000; Schieber, 2001; Harris et al., 2018). For example, the stratigraphic variability of the distribution of organic macerals is illustrated by the observation that in the New Albany Shale and Chattanooga Shale, alginite derived from *Tasmanites* cysts is concentrated at maximum flooding surfaces (MFSs) (Schieber, 2001; Lazar, 2007).

The Upper Devonian New Albany Shale of the Illinois Basin is an organic-rich formation with TOC contents ranging from <1% to 20% (Chou et al., 1991), and its thermal maturity ranges from vitrinite reflectance (R_o) 0.5% near the basin margin to 1.5% at Hicks Dome, Illinois (Strąpoć et al., 2010; Mastalerz et al., 2013). Although geochemically OM in the New Albany Shale is classified as type II kerogen on the basis of Rock-Eval pyrolysis (Chou et al., 1991; Akar et al., 2015), it is nonetheless composed of varying organic macerals including amorphous organic matter (AOM), alginite, liptodetrinite, vitrinite, inertinite, and solid bitumen (SB) when examined with a reflected-light microscope (Mastalerz et al., 2012, 2013; Wei et al., 2016; Liu et al., 2017, 2019). Commercial oil and gas production from the New Albany Shale has been reported where it has oil-window maturity (Hamilton-Smith et al., 1994; Nuttall et al., 2015).

Lazar (2007) studied the controls of paleo-redox conditions, paleoproductivity, and clastic dilution on organic matter accumulation in each unit of the New Albany Shale. Because Lazar (2007) only had TOC contents available, he operated under the assumption of uniform marine OM, although he noted that petrographic examination of these rocks shows considerable variability in the relative abundances of organic macerals (also pointed out by Mastalerz et al. (2012, 2013) and Liu et al. (2017, 2019)) and that quantitative information on their abundances could affect the conclusions reached in his study. This study builds on the earlier work of Lazar (2007) and adds to the data set with more detailed information on the stratigraphic variation of TOC content, and augments it with newly acquired data on the types and proportions of organic macerals. The goal of this investigation is to understand the controls on TOC content from a perspective of organic maceral accumulation in the sequence stratigraphic context of the Upper Devonian New Albany Shale of the Illinois Basin. Specific objectives are to: (1) document TOC content distribution in greater detail; (2) reevaluate the influence of relative sea-level fluctuations on paleoproductivity, clastic supply, bottom-water redox conditions, and their combined control on OM accumulation; and (3) examine the stratigraphic variability of organic macerals (AOM, alginite, vitrinite, and inertinite) within the New Albany Shale. Results of this study should allow for more sophisticated assessment of OM accumulation in time-equivalent Upper Devonian black shales deposited in adjacent epicontinental basins such as the Ohio Shale of the central Appalachian Basin, the Antrim Shale of the Michigan Basin, the Chattanooga Shale of the southern Appalachian Basin, and the Bakken Shale of the Williston Basin (Schieber, 1998; Schieber and Lazar, 2004).

2. Geological background

The Upper Devonian New Albany Shale of the Illinois Basin was deposited in an epicontinental sea during the late Devonian (Lineback, 1964, 1968; Beier and Hayes, 1989). It unconformably overlies the Middle Devonian North Vernon Limestone and underlies the Falling Run Bed, a phosphatic lag deposit (Campbell, 1946). Where the Falling Run Bed is absent, it is unconformably overlain by the early Mississippian Underwood, Henryville, and Jacobs Chapel Beds, or directly overlain by the Mississippian Rockford Limestone or the Mississippian New Providence Shale if these beds are absent (Campbell, 1946; Lineback, 1964, 1968). The New Albany Shale is composed of the Blocher, Selmier, Morgan Trail, Camp Run, and Clegg Creek Member in ascending order (Lineback, 1964, 1968). Lithologically, the New Albany Shale is composed of black laminated to banded shales and greenish-gray, bioturbated shales (Lineback, 1964, 1968; Lazar, 2007).

A complete New Albany Shale core of 39.43 m thickness that was described by Lazar (2007) for a sequence stratigraphic study, has been further examined and analyzed in order to study the distribution of TOC and organic macerals within a sequence stratigraphic context. The core is from Daviess County, Indiana (Fig. 1) with a coordinate of X = 494,611, Y = 4,276,705 (North American Datum 83; Lazar, 2007). The core (1–3 Kavanaugh) was drilled by Deka Exploration Inc. in 1994. OM in this core indicates a thermal maturity of 0.55% R_o. Being marginally mature, OM in this core has not undergone significant thermal transformation, although early diagenesis could to some degree alter OM through chemical and microbial degradation (Curtis, 1980; Tissot and Welte, 1984).

Using the conceptual framework of Schieber (1998) and Schieber and Lazar (2004), the studied New Albany Shale core can be divided into four basin-wide depositional sequences based on integration of sedimentological, paleontological, geophysical, and geochemical data (Fig. 2) (Lazar, 2007). Within those sequences, we identified six major lithofacies based on sedimentological (color, lamination, and banding) and ichnological (bioturbation intensity) characteristics: (1) black laminated to banded carbonate-bearing shale, (2) black laminated to banded shale, (3) black to brownish laminated shale with abundant lag deposits, (4) black-gray cyclic shale, (5) black massive to banded shale with interbedded gray bioturbated shale, and (6) black massive to banded shale (Fig. 3).

The black laminated to banded carbonate-bearing shale lithofacies (Figs. 2, 3A) is limited to unit 1TST (TST of sequence 1) with varying content of carbonate minerals (calcite and dolomite) and a bioturbation index (BI) of 0–1. The laminae are mainly composed of silt-sized quartz and recycled dolomite (Fig. 4) and formed through intermittent reworking of bottom sediments by storms and waves which winnowed the seabed and removed the fine-grained fraction (e.g., clay minerals and clay-sized particles). The black laminated to banded shale lithofacies (Figs. 2, 3B) is most common in units 1HST (BI = 0–2) and 3TST (BI = 0–1). The black to brownish laminated shale with abundant lag deposits (Figs. 2, 3C) is the major lithofacies in units 2LST (lowstand systems tract, BI = 0–1) and 4LST (BI = 0–2). Laminae and lag deposits, which can be cm-thick, formed via intensive reworking of bottom sediments by strong storms and waves (Schieber, 1998). The brownish color is due to an abundance of pyrite and *Tasmanites* microfossils, unicellular green algae that belong to the class Prasinophyceae (Tappan, 1980). The black-gray cyclic shale lithofacies (Figs. 2, 3D) occurs in the upper half of unit 2TST (BI = 2–4) and the entire 2HST (BI = 3–4). The formation of these black-gray cyclic shales has been interpreted to reflect alternation of anoxic and oxic environments resulting from fluctuations of relative sea level (Calvert et al., 1996). As such the black-gray cycles most likely represent distal parasequences (Schieber,

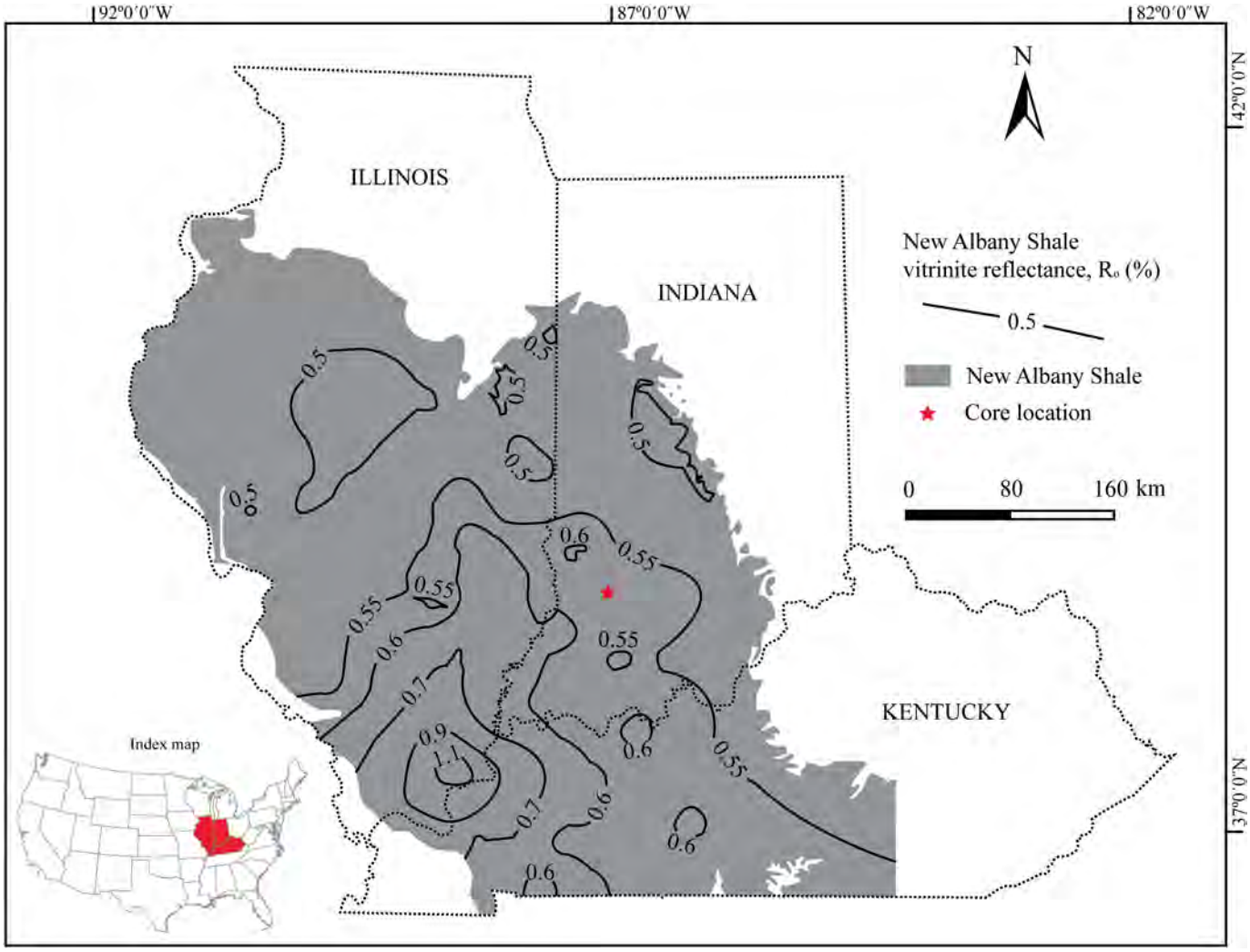

Fig. 1. Map showing the location of the drill core and the extent of the New Albany Shale. Vitrinite reflectance isolines are from Mastalerz et al. (2013).

1998) that reflect a high-frequency interplay of sediment buildup (shallowing) and intermittent small increases of sea level (deepening) as detailed by Spencer (2013). The black massive to banded shale with interbedded gray bioturbated shale lithofacies (Figs. 2, 3E−F) is restricted to unit 3HST (BI = 0–2). Gray bioturbated beds are organic-poor beds. The black massive to banded shale lithofacies (Figs. 2, 3G) is common in units 4TST (BI = 0–1) and 4HST (BI = 0–1). Generally, shales deposited in HSTs are more intensively bioturbated than those in TSTs within a given depositional sequence.

3. Analytical methods

Portable x-ray fluorescence (pXRF) instrumentation can provide rapid, non-destructive, and quantitative geochemical analysis of mudstone samples (Rowe et al., 2012). Major and trace elements in 482 samples were measured on the core at a spacing of approximately 8 cm with a pXRF analyzer (Thermo Niton XL3t GOLDD+) at the Indiana Geological and Water Survey. The measurements were carried out in situ on the cleaned surfaces of core slabs and conducted on a round area with a diameter of 11 mm. The pXRF analyzer was run in "Test All Geo" mode for 75 s. Three USGS certified reference materials (one carbonatite and two shale: COQ-1, SDO-1, and SBC-1) were analyzed at the beginning and end of each analytical session to examine the accuracy and precision of the analyses (McLaughlin et al., 2016). In this study, the analysis errors for major elements silicon (Si), aluminum (Al), titanium (Ti), phosphorus (P) are 0.78%, 2.88%, 3.27%, and 8.49%, respectively. Errors for trace elements molybdenum (Mo), nickel (Ni), vanadium (V), U, thorium (Th), and cobalt (Co) are 13.24%, 21.24%, 23.31%, 34.71%, 38.43%, and 43.17%, respectively, which are much higher than those of major elements.

Because portable XRF spectrometers have a lower detection accuracy than high-energy XRF spectrometers, contents of elements Si, Al, Ti, P, U, Mo, V, Ni, Th, and Co obtained with pXRF analyzer were calibrated with 44 previously analyzed New Albany Shale samples from Lazar (2007) (Supplementary Fig. 1). Major elements Si, Al, and Ti and trace elements U, V, and Mo exhibit high regression coefficients of determination ($R^2 > 0.7$), whereas coefficients of determination for P and trace elements Ni, Th, and Co are relatively low (Supplementary Fig. 1). Although accuracy is low, trace element ratio profiles can still indicate stratigraphic trends of paleo-redox conditions. Because U is commonly associated with OM in marine shales (Swanson, 1960; Leventhal, 1981; Fertl and Chilingar, 1988; Bohacs and Schwalbach, 1994; Lüning and Kolonic, 2003), the TOC content of the 482 samples was calculated based on the relationship between TOC and U content (Eq. (1)) established with 43 previously analyzed New Albany Shale samples (Lazar, 2007). This relationship is very similar to the results of Fertl and Chilingar (1988) (Fig. 5).

$$\mathrm{TOC\ (wt\%)} = 4.18\ \ln\mathrm{U(ppm)} - 6.26 \quad (1)$$

The TOC content of seventeen samples was measured using a LECO elemental analyzer (SC832DR). The seventeen samples were selected to

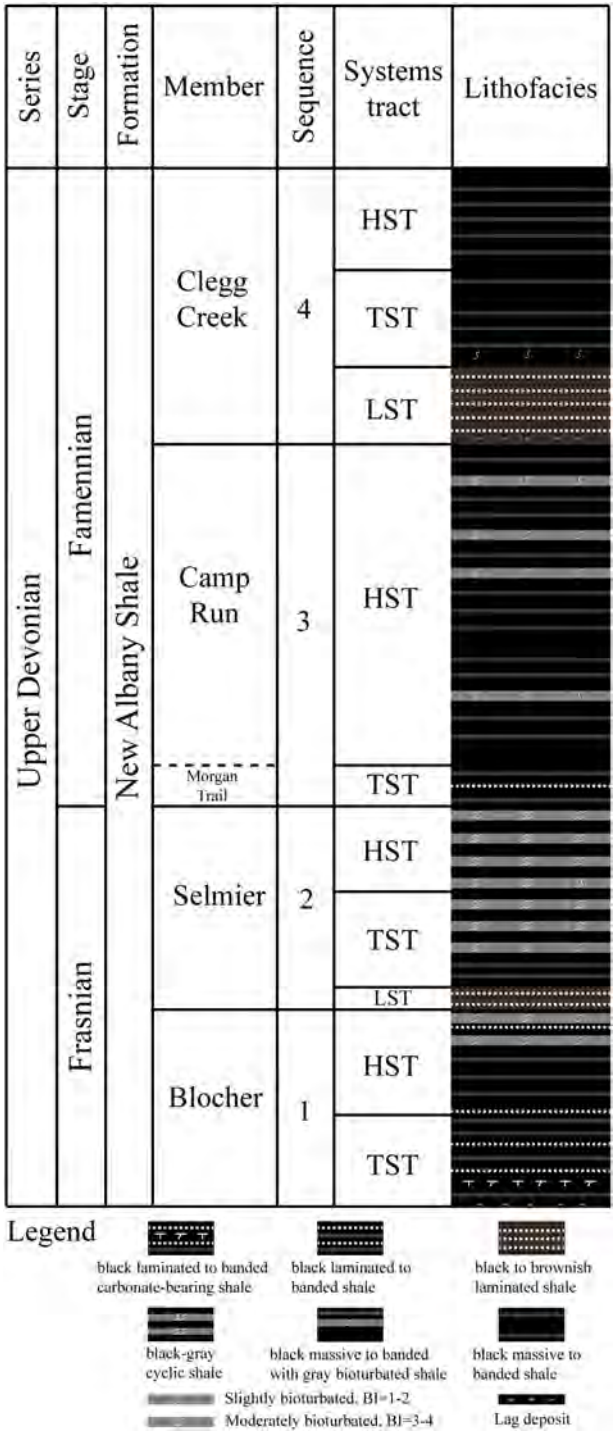

Fig. 2. Sequence stratigraphic framework of the New Albany Shale. Modified from Lazar (2007).

supplement the forty-four measurements of Lazar (2007) from the same core and to cover the unmeasured intervals. During the TOC measurements, 0.25 g powdered samples were acidified to remove carbonate minerals and then combusted in the LECO elemental analyzer. The amounts of generated CO_2 were converted to organic C content in samples. A duplicate sample was measured to ensure the accuracy of measurements. Of the 61 samples (17 in this study and 44 from Lazar (2007)) with TOC contents, thirty-three samples were taken from ten systems tracts in four depositional sequences for organic petrographic study. Vitrinite reflectance of shale samples was measured on polished whole-rock pellets using a Zeiss RS-III microscope with 50 measurements. Semi-quantitative organic petrographic compositions (AOM, alginite, liptodetrinite, vitrinite inertinite, and SB) of shale samples were determined via point-counting (500 points counted only on OM). The maceral groups vitrinite and inertinite were not classified into macerals because of their scarcity. The liptinite group includes AOM, alginite, and liptodetrinite because they are dominant oil-prone macerals in the New Albany Shale (Liu et al., 2017, 2019) and marine black shales in general (Mastalerz et al., 2018). Organic macerals were identified and photographed using a reflected-light microscope (Leica DFC310 FX) in reflected white light (for occurrence, color, and morphology) and blue light (for fluorescence properties) with oil immersion. A field emission scanning electron microscope (FEI Quanta 400 FEG) was used to examine shale composition and AOM using a correlative microscopy approach (reflected-light and SEM microscopy). The methods of correlative microscopy have been presented in Liu et al. (2017).

4. Results

4.1. Stratigraphic variation of TOC content

The TOC content of the New Albany Shale measured in this study ranges from 0.18% to 16.29%, with an average content of 6.53% (Fig. 6). Samples with the same lithofacies and next to each other show high variations of TOC content (e.g., at 630.75 m; Fig. 6), suggesting high heterogeneity of organic richness in black shales. The Clegg Creek Member (sequence 4) exhibits the highest TOC content (average TOC content 8.22%) in the New Albany Shale. Within a given depositional sequence, TOC content increases in the TST, reaches a maximum before getting to the MFS, and maintains relatively low values during the HST (Fig. 6). Stratigraphically, the TOC profile displays a very similar trend to the gamma-ray profile except in the Blocher Member (Fig. 6).

Calculated TOC content with Eq. (1) ranges from 0 to 12.53%, with an average content of 6.45%, which is very close to the measured average TOC content of 6.53%. The calculated TOC profile is very similar to the measured TOC profile and closely matches the gamma-ray profile (Fig. 6), suggesting that U is the main contributor to gamma radiation in the New Albany Shale. As with the trend of measured TOC in the sequence stratigraphic context, calculated TOC content increases in the TST, reaches a maximum before getting to the MFS, and maintains relatively low values during the HST with the exception of the Blocher Member (Fig. 6). Similar to the gamma-ray profile, the calculated TOC content is relatively constant in the Blocher Member (Fig. 6).

4.2. Paleoproductivity

Even though the New Albany Shale is characterized by high clay content (Mastalerz et al., 2013), there is a significant contribution of biogenic silica (Schieber, 1996; Schieber et al., 2000). Biogenic silica in the New Albany Shale is primarily sourced from radiolaria, planktonic organisms with an opaline test (Schieber, 1996; Schieber et al., 2000). High biogenic silica content (Si_{bio}) typically indicates high paleoproductivity (Ross and Bustin, 2009), and for this study Si_{bio} content was calculated using the following formula (Eq. (2); Ross and Bustin, 2009):

$$Si_{bio} = Si_{sample} - \left[(Si : Al)_{background} \times Al_{sample}\right] \quad (2)$$

A Si:Al ratio of 2.55 is used as the background value, which is the lowest Si:Al ratio (at 623.90 m) in the New Albany Shale. This interval is gray bioturbated shale and is mainly composed of detrital components, such as clay minerals (mostly illite), silt-sized quartz, dolomite, albite, potassium (K)-feldspar and minor pyrite, muscovite, and biotite (Fig. 7). Biogenic silica is very rare to absent in this interval. A background Si:Al ratio of 3.11 (Wedepohl, 1971) has been used in many previous studies (Ross and Bustin, 2009; Dong et al., 2017; Zhao et al., 2017; Harris et al., 2018), but at that ratio, a large number of samples would

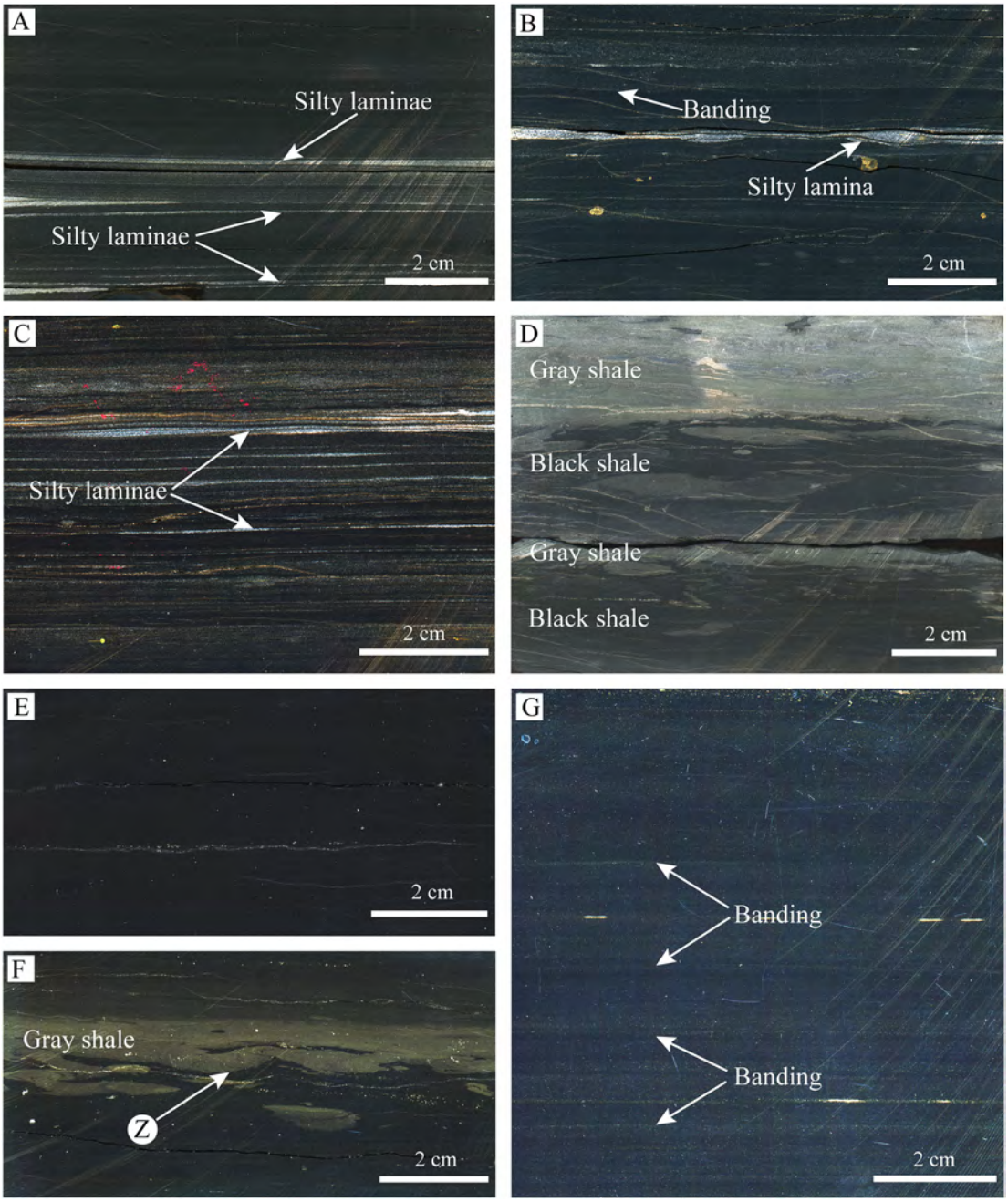

Fig. 3. Images of scanned core slabs showing major lithofacies in the New Albany Shale. (A) Black laminated to banded carbonate-bearing shale. (B) Black laminated to banded shale. (C) Black laminated shale. (D) Black-gray cyclic shale. (E) Black massive shale. (F) Black massive to banded shale with interbedded gray bioturbated shale. Note the *Zoophycos* burrow in the center. (G) Black massive to banded shale. Z = *Zoophycos*.

have negative Si_{bio} content. Because that is implausible, a background Si:Al ratio of 3.11 is considered too high for the New Albany Shale. Likewise, Harris et al. (2018) reported that a background Si:Al ratio of 3.11 would result in negative values for calculated biogenic silica in the Upper Devonian Duvernay Formation (Western Canada Sedimentary Basin). Given that the background Si:Al ratio of 3.11 is based on an average composition that includes data from a large number of shales across the globe and without differentiation of biogenic vs detrital sources of SiO_2 (Wedepohl, 1971), universal application of a Si:Al background ratio of 3.11 should be discouraged. As shown in this study, a plausible minimum Si:Al ratio that is intrinsic to a given stratigraphic interval can be derived and should help a more realistic assessment of biogenic silica inputs.

In the studied core, total Si content ranges from 4.07 to 38.90% (average 25.52%), out of which 0 to 35.14% (average 6.01%) is calculated as of biogenic origin, suggesting that 24% of total Si is biogenic. Sequence 4 has the highest biogenic Si content (average Si_{bio} 9.51%) in the New Albany Shale (Fig. 6). The highest Si_{bio} (35.14%) content occurs near the MFS of sequence 4, accounting for 90% of total Si. Within a given depositional sequence, Si_{bio} content increases in the TST, reaches a maximum at the MFS, and decreases in the HST (Fig. 6).

Phosphorus is an essential nutrient for marine phytoplankton and all organisms in general (Schoepfer et al., 2015), and its content in marine sediments can be related to surface ocean productivity (Schenau et al., 2005). P content in the New Albany Shale core is relatively constant (close to 0.04%). P content in the Clegg Creek Member (average content

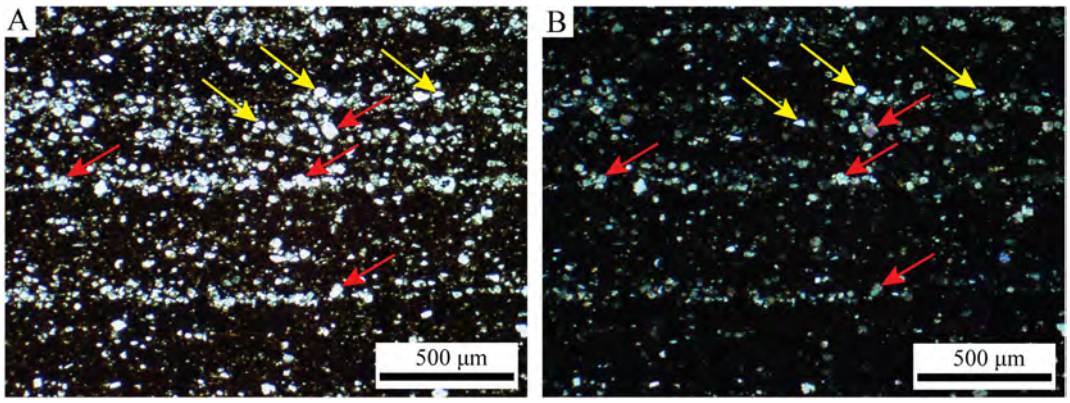

Fig. 4. Photomicrographs of silty laminae in the New Albany Shale. The laminae are composed of silt-sized quartz (yellow arrows) and recycled dolomite (red arrows). (A) Plane-polarized light; (B) cross-polarized light.

0.06%), however, is higher than in the rest of the core (average content 0.03%). The high P content at the bottom of unit 4LST results from the enrichment of reworked conodont fragments. The P profile shows a similar distribution pattern to the Si_{bio} profile, but the P content maximum at the MFS is not as clear as in the case of Si_{bio} (Fig. 6).

4.3. Clastic supply

Al is abundant in aluminosilicates such as clay minerals and feldspars, and Ti is contained in heavy minerals such as rutile (Brumsack, 2006). Al and Ti are chemically conservative during diagenesis (Brumsack, 2006) and have been used to serve as proxies for clastic supply (Sageman et al., 2003; Rimmer et al., 2004; Dong et al., 2017).

Al and Ti contents range from 0 to 10.20% (average 7.65%) and 0 to 0.56% (average 0.41%), respectively. Stratigraphically, Al and Ti contents display the same trend, and show an opposite distribution pattern compared to the Si_{bio} profile, with Al and Ti content at a minimum (but Si_{bio} maximum) at the MFS (Fig. 6). Within a given depositional sequence, Al and Ti contents decrease in the TST, reach a minimum at the MFS, and increase in the HST, with the exception of the Blocher Member (Fig. 6).

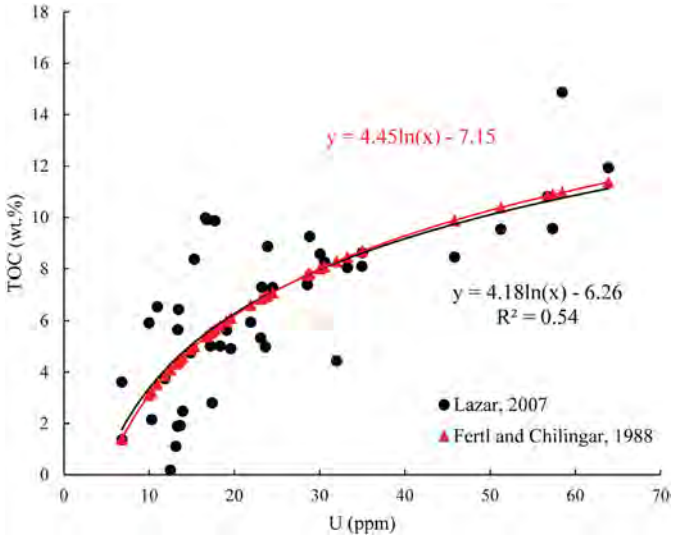

Fig. 5. Correlation between TOC and U content in the New Albany Shale and an empirical relationship between TOC and U content from Fertl and Chilingar (1988). TOC and U data of the New Albany Shale are from Lazar (2007).

4.4. Bottom-water redox conditions

There is a variety of trace element-based geochemical proxies that have been suggested as indicators of relative oxygenation of bottom waters (e.g., Adams and Weaver, 1958; Hatch and Leventhal, 1992; Jones and Manning, 1994; Rimmer et al., 2004). These proxies, however, may provide contradictory results, and should not be applied rigidly (Rimmer, 2004; Rimmer et al., 2004; Lazar, 2007; Ocubalidet et al., 2018). Instead, they are best used as relative indicators of levels and trends of bottom-water oxygenation (Rimmer, 2004; Rimmer et al., 2004).

$U(UO_2(CO_3)_3^{4-})$ is soluble in seawater, but it will be converted to the less soluble U(UO_2, U_3O_7, or U_3O_8) in reducing environments (Langmuir, 1978; Anderson et al., 1989; Klinkhammer and Palmer, 1991; Algeo and Tribovillard, 2009; Cumberland et al., 2016). U(IV, +4 oxidation state) occurs in marine OM as either U dioxide (UO_2) in an absorbed state or as U-OM compounds (Swanson, 1960; Cumberland et al., 2016). Th is typically associated with heavy minerals and is relatively immobile during diagenesis (Adams and Weaver, 1958). Therefore, high U/Th ratios of marine sediments are generally thought to indicate oxygen-deficient conditions (Adams and Weaver, 1958; Jones and Manning, 1994).

In this study, the U/Th ratio profile closely matches the calculated TOC profile (Fig. 6). Stratigraphically, the U/Th ratio increases in the TST, reaches a maximum before the MFS, and maintains relatively low values during the HST. Most of the U/Th ratio values are higher than 0.75, which may indicate dysoxic to anoxic environments (Tyson and Pearson, 1991; Jones and Manning, 1994) (Fig. 6).

Enrichment factors (EF) have been used to evaluate the enrichment of trace metals in organic-rich shales relative to average shales (Brumsack, 2006; Tribovillard et al., 2006, 2012; Algeo and Tribovillard, 2009). EF are calculated as (Eq. (3)):

$$X_{EF} = \left[(X : Al)_{sample}/(X : Al)_{average\ shale}\right] \quad (3)$$

where X and Al represent the concentrations of elements X and Al, respectively. Samples were normalized using the post-Archean average shale (PAAS) composition (Taylor and McLennan, 1985).

U_{EF} ranges from to 0 to 50.08, with an average value of 11.26, suggesting a common anoxic environment (Algeo and Tribovillard, 2009; Tribovillard et al., 2012) during the deposition of the New Albany Shale. U_{EF} with values of 0 probably results from the relatively high detection limit of pXRF analyzer (samples with low U content were not detected). Stratigraphically, the U_{EF} profile displays the same distribution pattern as the U/Th profile (Fig. 6).

V and Ni are preferentially concentrated in tetrapyrrole compounds under anoxic conditions (Lewan and Maynard, 1982), and V/(V + Ni) ratios from whole-rock analyses have been used to indicate

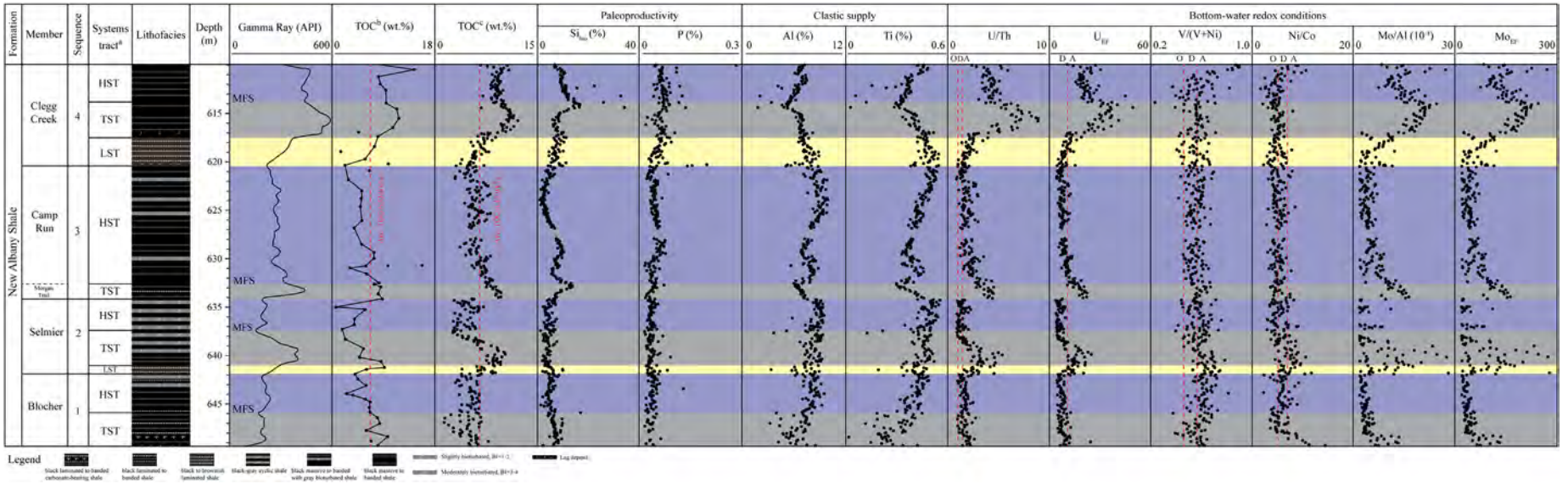

Fig. 6. Stratigraphic distribution of lithofacies and profiles of gamma-ray log, total organic carbon (TOC) content, and geochemical proxies of paleoproductivity, clastic supply, and bottom-water redox conditions of the New Albany Shale in the studied core. Proposed threshold values for the degree of bottom-water oxygenation are from Tyson and Pearson (1991); Hatch and Leventhal (1992); Jones and Manning (1994); Algeo and Tribovillard, 2009. LST = lowstand systems tract; TST = transgressive systems tract; HST = highstand systems tract; MFS = maximum flooding surface; O = oxic; D = dysoxic; A = anoxic. [a]Sequence stratigraphic context of the New Albany Shale is modified from Lazar (2007). [b]Measured TOC content of 17 samples in this study and 44 samples from Lazar (2007). [c]TOC content calculated from U content. pXRF data can be found in Supplementary data sets.

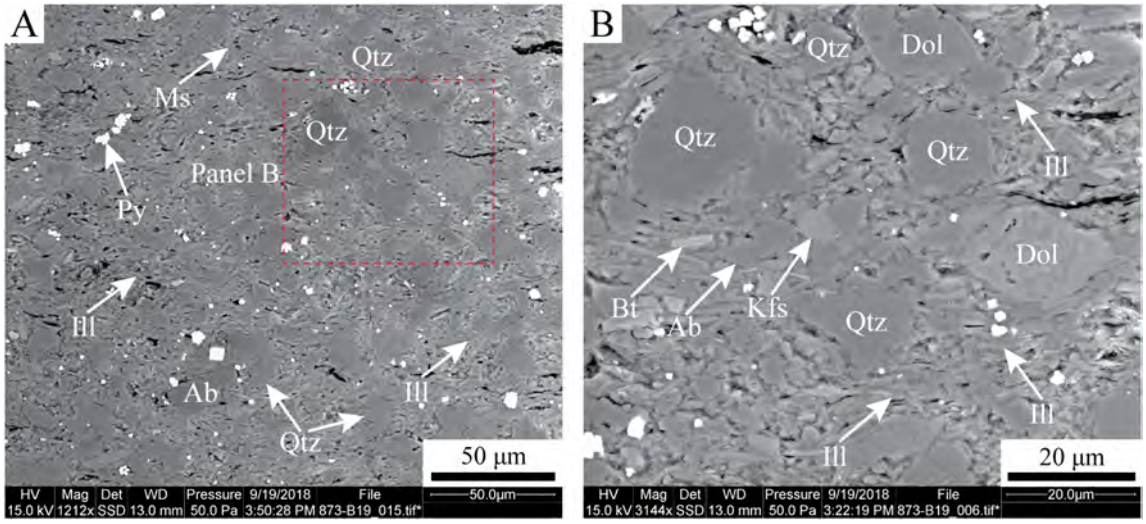

Fig. 7. SEM images (backscattered electron image) of shale sample with a Si:Al ratio of 2.55 at 623.90 m. The sample is composed of clay minerals (mostly illite), silt-sized quartz, dolomite, albite, K-feldspar and minor pyrite, muscovite, and biotite. Panel B is the close-up view of the red dashed framed area in panel A. Qtz = quartz; Dol = dolomite; Ab = albite; Kfs = K-feldspar; Py = pyrite; Bt = biotite; Ms. = muscovite; Ill = illite.

environmental conditions at the time of deposition (Hatch and Leventhal, 1992). For the studied interval, the V/(V + Ni) ratio does not show significant variations stratigraphically, and is generally higher than 0.46, suggesting dysoxic to anoxic conditions (Tyson and Pearson, 1991; Hatch and Leventhal, 1992) (Fig. 6).

Co is strongly determined by the abundance of clastic materials (Tribovillard et al., 2006), and the Ni/Co ratio of mudstones has been used to indicate oxygenation conditions (Jones and Manning, 1994). Similar to the V/(V + Ni) ratio, the Ni/Co ratio does not show significant variations stratigraphically (Fig. 6). Across the studied core, the Ni/Co ratio is typically lower than 7.00, which would suggest dysoxic to oxic conditions (Tyson and Pearson, 1991; Jones and Manning, 1994) (Fig. 6).

Mo tends to be enriched in marine sediments under anoxic conditions (Calvert and Pedersen, 1993; Algeo and Lyons, 2006; Tribovillard et al., 2006). Mo content is generally normalized to Al content to compensate for the dilution of biogenic minerals (common diluents are calcium carbonate and biogenic silica; Tribovillard et al., 2006), and this normalized Mo content has in the past been proposed as an indicator of paleo-redox conditions of marine black shales (Rimmer et al., 2004). In this study, the Mo/Al ratio and the U/Th ratio display similar distribution patterns stratigraphically except in sequence 4, where the Mo/Al ratio reaches a maximum at the MFS (Fig. 6). Covariation of U and Mo has been reported in modern and paleo- marine systems (Algeo and Tribovillard, 2009; Tribovillard et al., 2012). No threshold values have been proposed to define paleo-redox conditions based on the Mo/Al ratio. Mo_{EF} ranges from to 0 to 283.17, with an average value of 69.85. Mo/Al ratio and Mo_{EF} show exactly the same distribution pattern (Fig. 6) because Mo_{EF} is normalized with Al content.

4.5. Organic maceral variation

Organic macerals are microscopically recognizable individual constituents of OM (Stach et al., 1982; Taylor et al., 1998). Organic macerals observed in this study include AOM, alginite, liptodetrinite, vitrinite, inertinite, and SB (Fig. 8). In marine organic-rich shales, AOM and alginite are of marine origin (Kus et al., 2017), whereas vitrinite and inertinite are derived from terrestrial woody materials (Stach et al., 1982; Taylor et al., 1998). AOM, derived from microbially degraded phytoplankton, zooplankton, and bacterial biomass, refers to structureless OM in coals and organic-rich shales (Teichmüller, 1989; Taylor et al., 1998; Pacton et al., 2011; Kus et al., 2017). AOM commonly has small mineral inclusions, such as clay minerals and clay-sized particles (e.g., quartz, feldspar, and pyrite), suggesting its degradation origin (Fig. 9). Alginite in the New Albany Shale is mainly in the form of *Tasmanites* cysts (Fig. 8). Liptodetrinite occurs as small fluorescencing OM particles (Fig. 8E), and is likely of algal origin. SB is secondary OM generated from primary oil-prone macerals (Jacob, 1989; Mastalerz et al., 2018), such as AOM and alginite (Liu et al., 2019). A detailed petrographic study of OM in the New Albany Shale was presented in Liu et al. (2017, 2019).

OM in the New Albany Shale is dominated by either AOM or alginite (Table 1). The terrestrial OM (vitrinite + inertinite) content is <10% (Table 1). Vitrinite content is typically lower than inertinite content (Table 1) because inertinite is chemically inert and vitrinite is possibly partially oxidized during transport to the place of deposition (Wei et al., 2016; Liu et al., 2019). Because this core is at the early mature stage (0.55% R_o), relatively low but varying contents of SB were observed (Table 1). This SB likely results from thermal degradation of labile OM (Liu et al., 2019).

The organic petrographic composition of the New Albany Shale varies stratigraphically (Fig. 10). AOM dominates except in the unit 1HST, the Selmier Member (sequence 2), the unit 3TST, and the unit 4LST (Table 1; Fig. 10). Within sequences 1, 2, and 4, AOM content increases in the TST, reaches a maximum near the MFS, and decreases in the HST (Fig. 10). There is a slight decrease of AOM content at the MFS (Fig. 10). Because OM is dominated by alginite in the Selmier Member, the stratigraphic distribution pattern of AOM content is not as obvious as in sequence 1 and 4 (Fig. 10). Compared to other sequences, sequence 3 does not show an AOM content maximum near the MFS, but within the middle of the HST (Fig. 10). In contrast to AOM, alginite displays an opposite pattern stratigraphically (Fig. 10). Alginite can be enriched in certain intervals of the studied core. For example, alginite accounts for 83.1% of total OM in sample NAS-15, whereas samples above and below it are dominated by AOM (Table 1; Figs. 10, 11). Terrestrial OM (vitrinite + inertinite) content is relatively constant (~2.5% of total OM) throughout most of the studied core except at the top where terrestrial OM accounts for 6–10% of total OM (Table 1; Figs. 10, 12). Ripley et al. (1990) also reported a high abundance of terrestrial OM (6–14%) within the upper part of the Clegg Creek Member. The increase of terrestrial OM at the top of the New Albany Shale is accompanied by increasing Al and Ti contents (Figs. 6, 10).

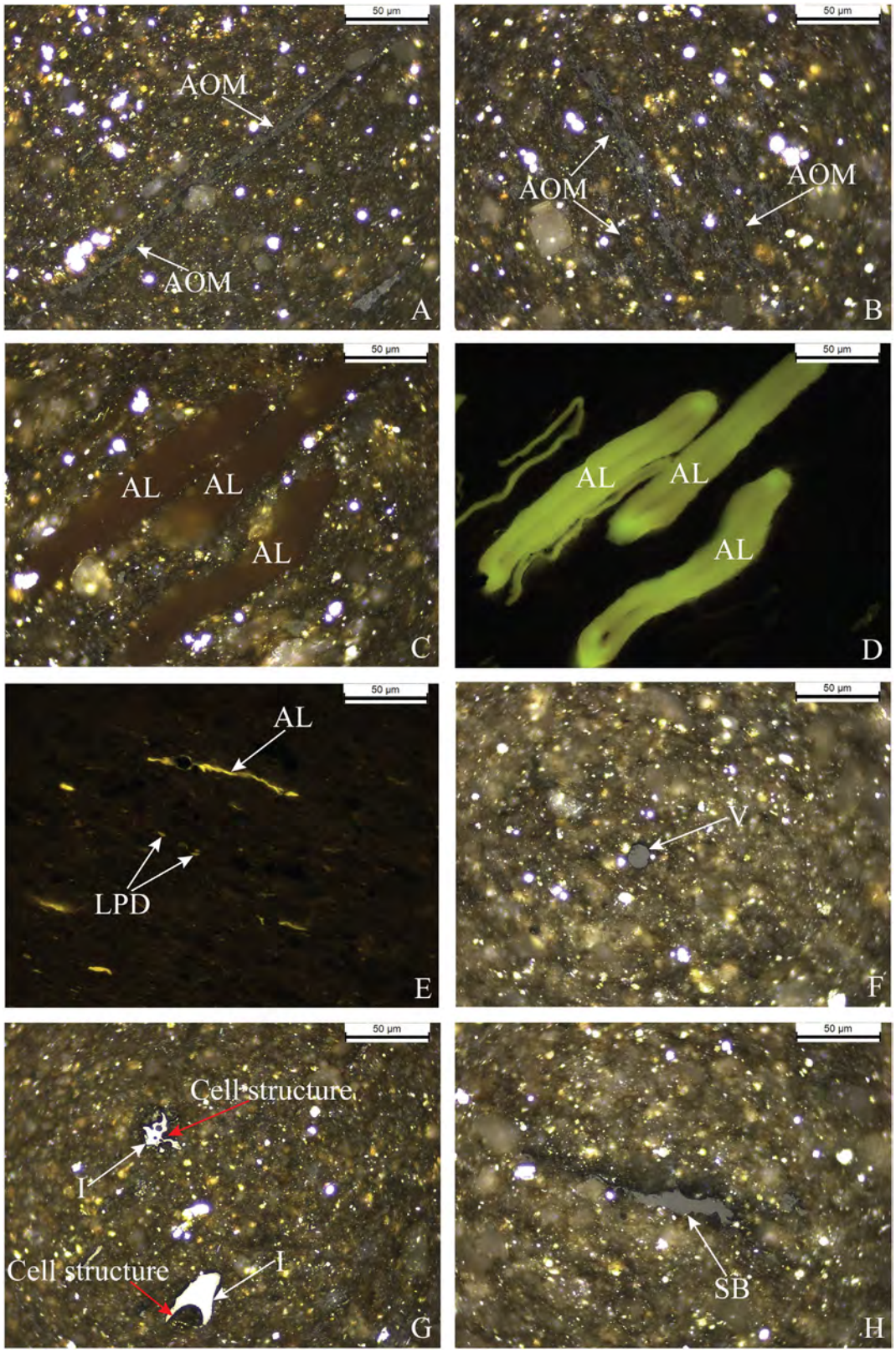

Fig. 8. Photomicrographs of organic macerals in reflected white light and oil immersion (A–C, F–H) and in fluorescence mode (D–E) in the New Albany Shale in the studied core. (A–B) Amorphous organic matter. AOM occurs as organic streaks. (C) Alginite in the form of *Tasmanites* cysts. The algal cysts are compacted. (D) The same field of panel C in fluorescence mode. Alginite shows greenish-yellow fluorescence at this maturity. (E) Liptodetrinite and alginite in fluorescence mode. (F–G) Vitrinite and inertinite occurring as dispersed particles in the matrix. Inertinite in panel G shows cellular structure (red arrows). (H) Solid bitumen. Note the embayments against mineral particles. AOM = amorphous organic matter; AL = alginite; LPD = liptodetrinite; V = vitrinite; I = inertinite; SB = solid bitumen.

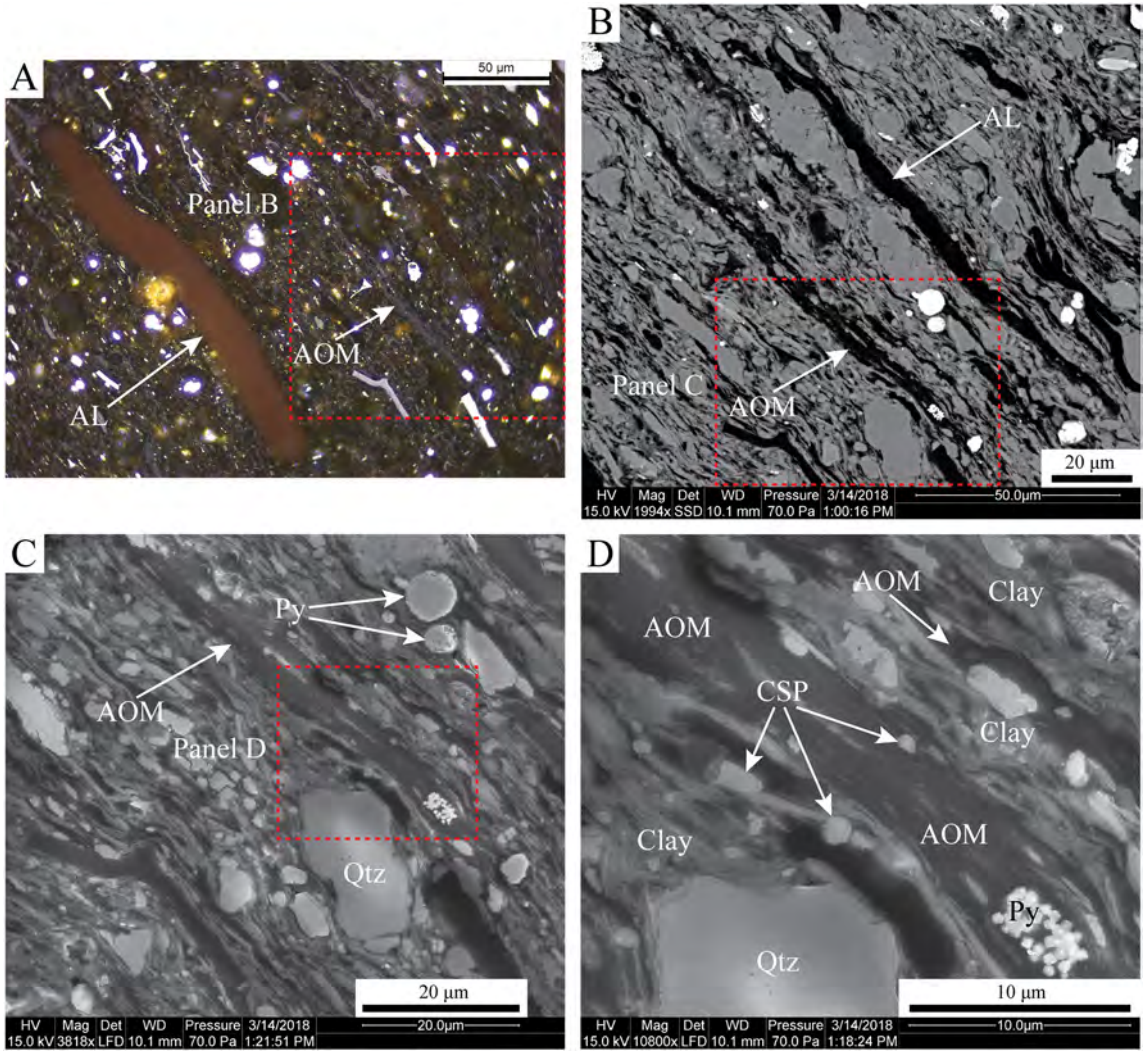

Fig. 9. Photomicrographs of AOM in the New Albany Shale in reflected white light and oil immersion (A) and its correlative SEM images (B, backscattered electron image; C–D, secondary electron images). AOM = amorphous organic matter; AL = alginite; Py = pyrite; Qtz = quartz; CSP = clay-sized particle.

5. Discussion

5.1. Paleoproductivity

OM preserved in marine sediments comes mainly from primary production of phytoplankton in the ocean (e.g., Müller and Suess, 1979; Schoepfer et al., 2015), together with a component of terrestrial OM supplied from adjacent land (e.g., Goñi et al., 1997; Hedges et al., 1997; Opsahl and Benner, 1997; Ponsaing et al., 2018). High paleoproductivity is favorable for enhanced OM burial (Pedersen and Calvert, 1990; Schoepfer et al., 2015). Biogenic silica content is considered a useful proxy for paleoproductivity (Ross and Bustin, 2009). Zhao et al. (2017) reported a positive correlation between TOC and excess (biogenic) silica content in the Wufeng and Longmaxi Formations of the Sichuan Basin (China). In this study, the Clegg Creek Member has the highest average Si_{bio} content (9.51%), P content (0.06%), and TOC content (8.22%) in the New Albany Shale (Fig. 6). High paleoproductivity could be one reason for high TOC content in the Clegg Creek Member, an assumption that is supported by the common presence of early diagenetic silica, derived from the dissolution of radiolaria (Schieber, 1996; Schieber et al., 2000), in *Tasmanites* cysts and microcrystalline quartz in the matrix in sequence 4 (Fig. 13). However, when abundant biogenic silica contributes to the shale composition, it can lower OM content in shales (Figs. 6, 13). Bohacs et al. (2005) and Passey et al. (2010) also suggested that primary productivity might have a dual impact on OM accumulation in organic-rich sediments, with organic-carbon-rich organisms enhancing OM content, but siliceous and calcareous organisms diluting OM content in sediments.

The stratigraphic distribution pattern of Si_{bio} content (Fig. 6) suggests increasing paleoproductivity in the TST and decreasing paleoproductivity in the HST. Lash and Blood (2011) and Dong et al. (2017) reported elevated diagenetic silica during the deposition of TSTs in the Devonian gas shales of the Appalachian Basin (USA) and the Middle and Upper Devonian Horn River Group of the Horn River Basin (Canada), respectively. The stratigraphic distribution pattern of Si_{bio} content, however, can alternatively be explained by decreasing clastic supply in the TST and increasing clastic supply in the HST (Fig. 6) with paleoproductivity held stable throughout a given sequence. Stratigraphically, the Si_{bio} profile displays an opposite distribution pattern relative to Al and Ti, with the Si_{bio} content maximum coinciding with the Al and Ti content minimum at MFSs (Fig. 6). Therefore, Si_{bio} variation in the New Albany Shale may not so much indicate paleoproductivity, but rather reflect changes of dilution by clastic materials (Fig. 6).

Mass flux of organic carbon per unit area (in g cm^{-2} kyr^{-1}) is a better way to represent the surface ocean productivity at the time of deposition of organic-rich sediments if a high-resolution chronostratigraphic framework is available (Algeo et al., 2011, 2013; Schoepfer et al., 2015). However, OM consumption during settling, early diagenesis, and thermal

Table 1
Sample depth, measured total organic carbon (TOC) content, and organic petrographic composition of the New Albany Shale in the studied core.

Sample	Depth (m)	TOC (wt.%)	Organic petrographic composition (volume %, on mineral-matter-free basis)					
			AOM	Alginite	Liptodetrinite	Vitrinite	Inertinite	SB
NAS-1	610.50	14.87	44.3	40.0	2.5	1.1	8.2	3.9
NAS-2	612.66	9.54	64.8	21.9	1.4	1.6	5.3	5.0
NAS-3	613.94	9.57	53.5	38.4	2.7	1.0	1.5	2.9
NAS-4	615.54	11.93	67.9	20.6	1.3	2.3	2.1	5.8
NAS-5	616.46	10.81	59.5	32.5	2.1	1.0	1.1	3.8
NAS-6	617.44	8.05	48.7	44.5	2.9	0.4	1.0	2.5
NAS-7	619.00	1.11	57.5	34.8	2.1	1.3	1.0	3.3
NAS-8	620.25	9.98	19.3	74.0	3.8	0.4	1.2	1.3
NAS-9	621.87	2.48	40.6	51.7	2.7	1.1	1.1	2.8
NAS-10	623.82	4.91	57.0	35.8	2.0	0.6	0.9	3.7
NAS-11	624.64	4.74	68.4	25.3	1.7	0.8	0.8	3.0
NAS-12	626.12	5.01	58.5	34.8	2.2	0.6	0.8	3.1
NAS-13	628.54	4.98	73.5	18.3	1.3	0.6	0.7	5.6
NAS-14	629.99	7.29	54.3	36.8	2.6	0.9	1.1	4.3
NAS-15	630.73	16.29	11.0	83.1	4.1	0.2	0.2	1.4
NAS-16	631.58	5.94	48.1	44.0	2.7	0.6	0.8	3.8
NAS-17	632.64	7.31	33.2	58.8	4.0	0.4	0.8	2.8
NAS-18	632.94	8.57	42.2	48.6	2.8	0.9	1.3	4.2
NAS-19	633.70	8.09	26.0	67.4	3.4	0.4	0.7	2.1
NAS-20	635.26	5.65	9.6	82.7	5.4	0.4	0.4	1.5
NAS-21	636.86	3.61	21.0	71.0	3.9	0.7	1.2	2.2
NAS-22	638.32	1.92	10.9	80.3	5.2	0.7	1.0	1.9
NAS-23	639.36	5.32	22.0	71.0	4.1	0.4	0.6	1.9
NAS-24	640.21	4.58	25.7	65.9	3.3	0.4	1.0	3.7
NAS-25	640.64	8.62	21.6	69.6	4.2	0.7	1.5	2.4
NAS-26	641.49	5.91	16.0	70.8	4.7	0.9	4.2	3.4
NAS-27	643.10	5.82	19.8	70.6	4.4	0.6	2.0	2.6
NAS-28	644.10	3.33	45.8	46.7	3.1	0.4	2.5	1.5
NAS-29	644.80	6.59	32.5	57.6	3.7	0.9	2.7	2.6
NAS-30	645.84	6.54	72.9	14.7	1.9	0.8	1.1	8.6
NAS-31	646.97	8.37	70.0	15.1	2.4	0.8	3.7	8.0
NAS-32	648.30	9.87	68.6	15.8	2.1	1.0	4.7	7.8
NAS-33	648.83	6.76	64.6	27.8	2.1	0.2	1.5	3.8
Average		7.10	43.3	47.6	3.0	0.8	1.8	3.6

AOM = amorphous organic matter; SB = solid bitumen.

maturation has to be carefully considered when calculating the primary productivity of phytoplankton in the ocean (Bralower and Thierstein, 1987; Raiswell and Berner, 1987; Tyson, 1995; Bohacs et al., 2005). The calculated primary productivity of OM during deposition of the New Albany Shale based on multiple sedimentologic, petrographic, and geochemical data, ranges from 10.1 to 952.4 mg C cm^{-2} kyr^{-1} with an average value of 155.4 mg C cm^{-2} kyr^{-1} (Lazar, 2007). No stratigraphic distribution pattern of primary productivity of OM exists in the New Albany Shale.

5.2. Clastic supply

Devonian clastics in the Illinois Basin were supplied from the east, the Acadian orogeny (Dickinson et al., 1983; Ettensohn, 2008; Schieber, 2016). The sedimentation rate of the studied New Albany Shale interval is extremely low (~ 0.24 cm/ka; Lazar, 2007). Relative sea-level fluctuations played a significant role in transporting detrital materials to the Illinois Basin. Generally speaking, detrital materials are restricted landward during transgressions and transported to the basin during regressions. The stratigraphic distribution patterns of Al and Ti contents (Fig. 6) suggest decreasing clastic supply in the TST and increasing clastic supply in the HST. The TOC profile exhibits an opposite trend compared to the Al and Ti profiles (Fig. 6), which indicates that clastic supply is not favorable for OM accumulation due to dilution. However, a too low clastic supply can imply limited supply of nutrients (e.g., N, P, Si, and Fe) to the basin, which in turn can reduce paleoproductivity (Killops and Killops, 2005). In addition, low clastic supply limits the burial of OM by clastic materials and thus keeps OM within the surficial zone of active microbial degradation for longer time intervals (Bohacs et al., 2005). Therefore, similar to paleoproductivity, clastic supply has a dual impact on OM accumulation in marine organic-rich sediments. What is worth noting is that Al and Ti contents (in %) may not represent the real flux of silisiclastic detritus because of the dilution of biogenic minerals (Tribovillard et al., 2006). However, Al and Ti contents correlate well with the sequence stratigraphic framework of the New Albany Shale (Fig. 6) proposed by Lazar (2007), and high Al and Ti contents typically indicate high sedimentation rate and possibly high detrital flux.

Al and Ti contents in the Blocher Member display a different pattern from the other three sequences (Fig. 6), which show decreasing Al and Ti contents in the TST and increasing Al and Ti contents in the HST with the minimum at the MFS. The reason for this difference could be that when sea level started to rise during the deposition of the Blocher Member, clastic materials were not yet effectively delivered to the basin (Brett et al., 2004). The Blocher Member contains calcareous fossil fragments and recycled (clastic) dolomite, as shown by laminae composed of *Tentaculites* and recycled dolomite (Fig. 14), which are features uncommon in the other three sequences.

5.3. Bottom-water redox conditions

The preservation potential of OM decreases in the presence of oxygen due to microbial degradation (Wignall, 1991). Nonetheless, OM can still be preserved if paleoproductivity is high enough (Pedersen and Calvert, 1990). The stratigraphic distribution of redox-sensitive trace element ratios suggests that paleo-redox conditions varied during the deposition of the New Albany Shale (Beier and Hayes, 1989; Lazar, 2007; Ocubalidet et al., 2018) (Fig. 6). The U/Th and V/(V + Ni) ratios suggest common dysoxic to anoxic conditions, whereas the Ni/Co ratio suggests common dysoxic to oxic conditions (Fig. 6). Previous studies have proposed that application of trace element ratios to indicate paleo-redox conditions should be in a relative sense, rather than strictly applying proposed thresholds (Rimmer, 2004; Rimmer et al., 2004;

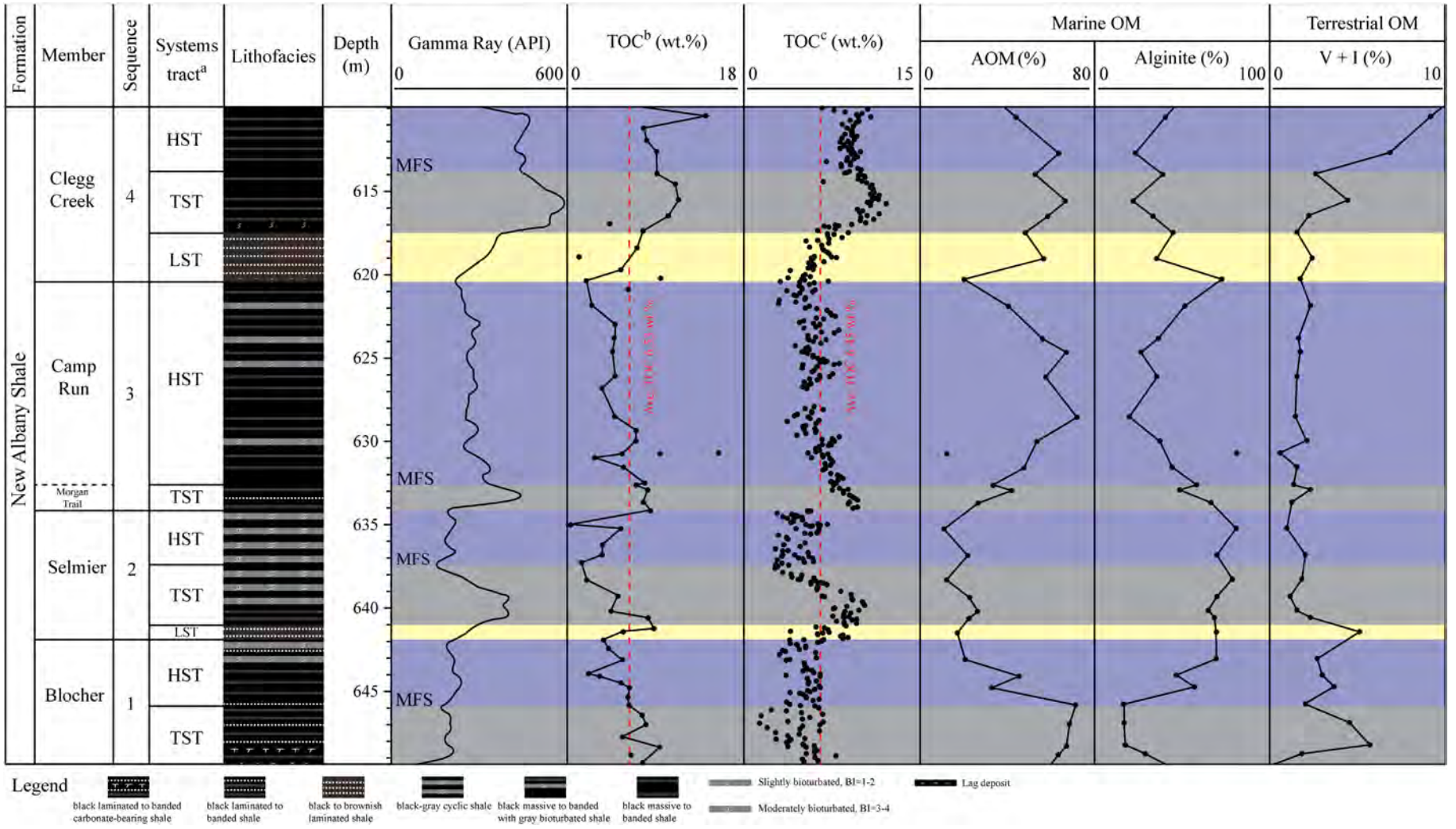

Fig. 10. Stratigraphic distribution of lithofacies, gamma-ray intensity, total organic carbon (TOC) content, and organic petrographic composition of the New Albany Shale in the studied core. LST = lowstand systems tract; TST = transgressive systems tract; HST = highstand systems tract; MFS = maximum flooding surface; OM = organic matter; AOM = amorphous organic matter; V = vitrinite; I = inertinite. [a]Sequence stratigraphic context of the New Albany Shale is modified from Lazar (2007). [b]Measured TOC content of 17 samples in this study and 44 samples from the same core (Lazar, 2007). [c]TOC content calculated from U content.

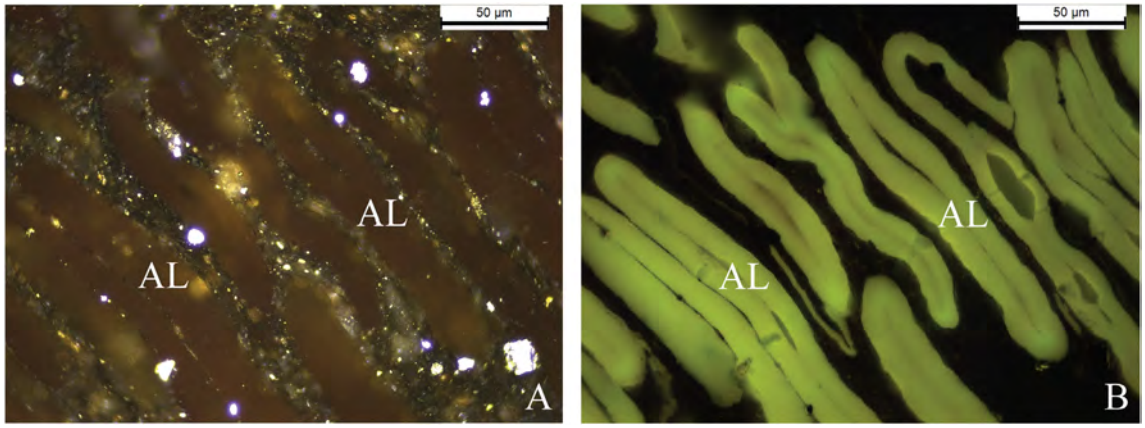

Fig. 11. Photomicrographs of alginite derived from *Tasmanites* cysts in reflected white light and oil immersion (A) and in fluorescence mode (B) in sample NAS-15. AL = alginite.

Lazar, 2007; Ocubalidet et al., 2018). For example, Ocubalidet et al. (2018) reported that the Ni/Co ratio indicates higher oxygenated conditions than the V/(V + Ni) ratio in the New Albany Shale. Based on geochemical and petrographic paleo-redox proxies and sedimentologic observations from cores and thin sections, Lazar (2007) concluded that bottom water was mainly dysoxic with intermittent anoxia and oxic conditions during the deposition of the New Albany Shale. Schieber (2009) also reported a common presence of agglutinated benthic foraminifera in the New Albany Shale, suggestive of bottom-water oxygenation.

V/(V + Ni) and Ni/Co ratios are relatively constant stratigraphically (Fig. 6) and thus of limited use for detecting variable paleo-redox conditions of bottom waters in this study. Because U_{EF} and Mo_{EF} profiles show the same distribution patterns as U/Th and Mo/Al profiles, respectively (Fig. 6), they will not be discussed separately. The stratigraphic distribution of U/Th and Mo/Al ratios indicates that oxygen content in bottom water decreases towards the MFS with the rise of sea level and increases towards the sequence boundary with the drop of sea level (Fig. 6). Interestingly, according to the U/Th and Mo/Al ratio profiles, the most oxygen-deficient condition (as indicated by metal ratios) does not occur at the MFS where relative sea level is presumed at a maximum (Fig. 6). A potential explanation for this could be that at the MFS strong storms that reworked the substrate and generated lag deposits at MFSs (Fig. 15) were able to supply oxygen to bottom waters via water column mixing. Because redox-sensitive metals would have been mobilized very close to the sediment-water interface under these conditions, they could have diffused out of the sediments into the overlying water (Shaw et al., 1994; Morford and Emerson, 1999). The mismatch between the U/Th and Mo/Al ratios at the MFS of sequence 4 (Fig. 6) is difficult to explain, probably due to the difference between the degree of enrichment of authigenic U and Mo (Algeo and Tribovillard, 2009; Tribovillard et al., 2012). The lag deposits at the MFS are mainly composed of pyrite, recrystallized radiolaria, *Tasmanites* cysts filled with authigenic quartz and pyrite, and microcrystalline quartz in the matrix (Figs. 13, 15). The *Tasmanites* cysts with authigenic infills suggest extremely low sedimentation rate (Schieber, 1996), otherwise the algal cysts would be compacted (Figs. 8C—D, 11). The U/Th and Mo/Al ratio profiles display a similar trend to the TOC profile (Fig. 6), suggesting that oxygen-deficient conditions are favorable for OM accumulation.

The U/Th and Mo/Al ratios indicate lower bottom-water oxygenation in the Clegg Creek Member compared to the other members, which could be another reason for high TOC content in the Clegg Creek Member besides high paleoproductivity (Fig. 6). A productivity-anoxia feedback (Ingall et al., 1993) may have contributed to OM accumulation during the deposition of the Clegg Creek Member (Ocubalidet et al., 2018). In the Blocher Member, the U/Th and Mo/Al ratios are relatively constant and close to the values in the HSTs of sequences 2 and 3 (Fig. 6). A potential explanation could be that relative sea level was still low during the deposition of the Blocher Member and bottom waters were still oxygenated to some extent because storms and waves, as indicated by silty laminae and lenses (Figs. 14, 16), would mix oxygen-deficient bottom waters and oxygenated surface waters. U and Mo do not tend to be enriched under such conditions (Langmuir, 1978; Anderson et al., 1989; Klinkhammer and Palmer, 1991; Calvert and Pedersen, 1993; Tribovillard et al., 2006; Algeo and Tribovillard, 2009); a possible explanation of low gamma-ray intensities observed in the Blocher Member (Fig. 6). Ocubalidet et al. (2018) also suggested that the paleoenvironment was dysoxic to oxic during the deposition

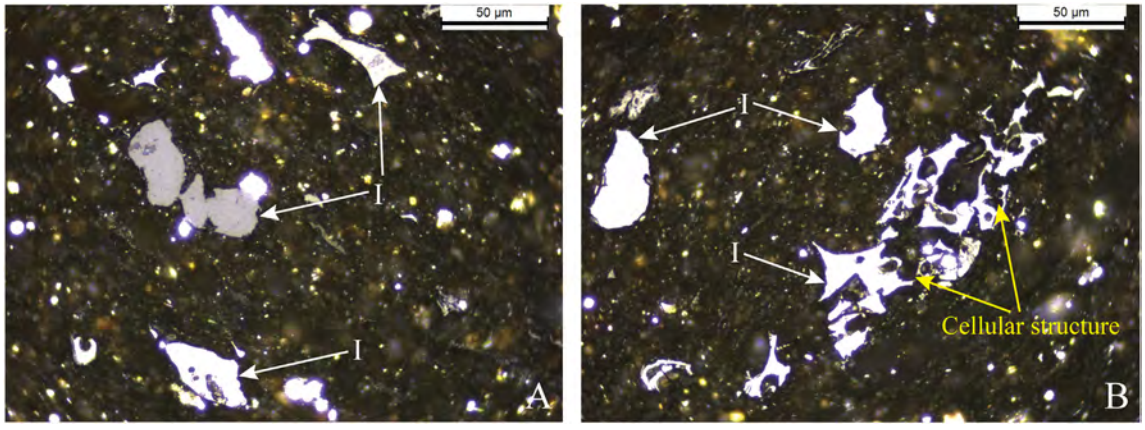

Fig. 12. Photomicrographs of inertinite in reflected white light and oil immersion in sample NAS-1. Inertinite in panel B shows cellular structure (yellow arrows). The cellular pores are filled with minerals. I = inertinite.

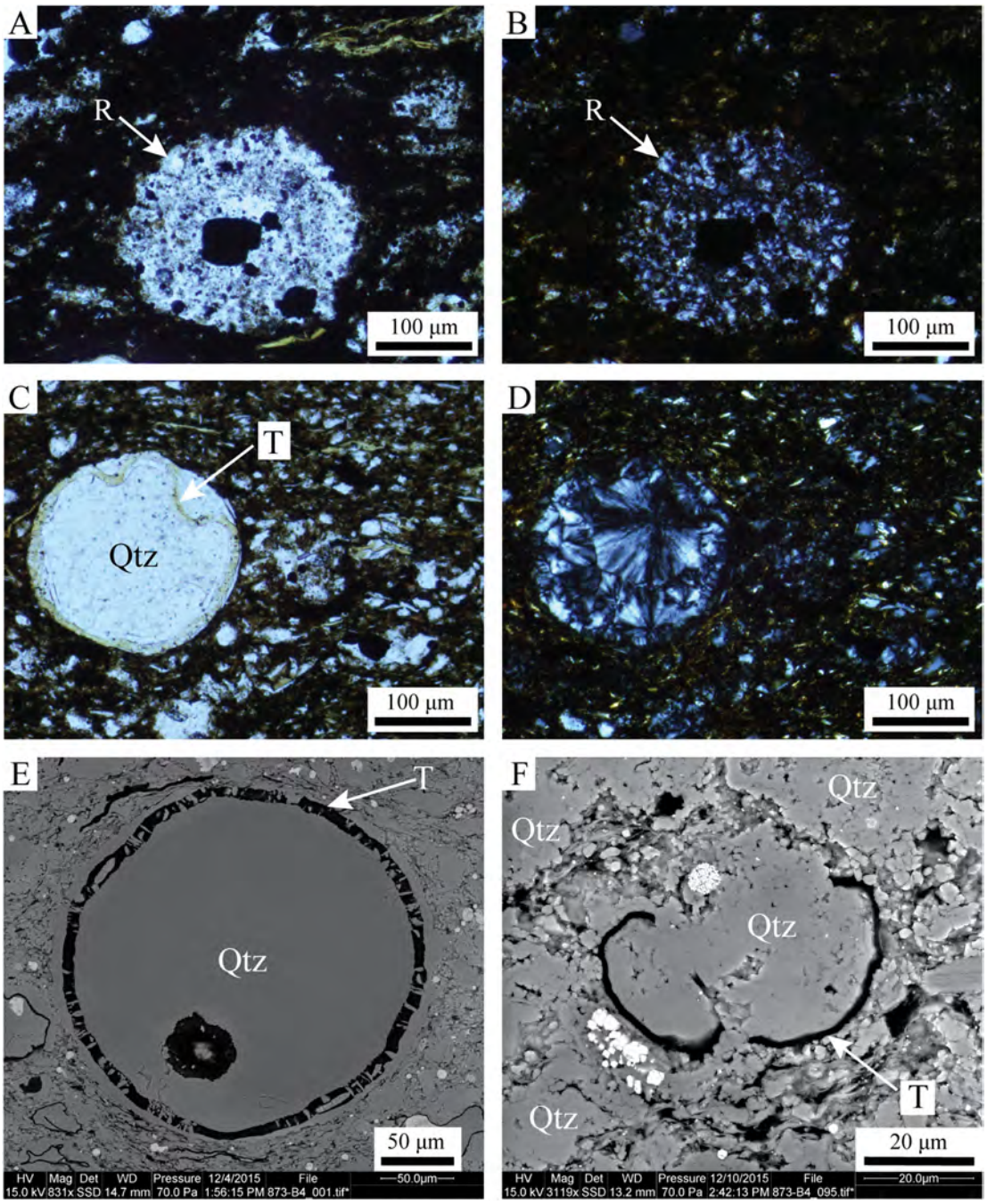

Fig. 13. Photomicrographs of biogenic silica in samples near the MFS of sequence 4 at 613.85 m. (A) Recrystallized radiolaria. The impurity results from inclusions of clay minerals and pyrite during silica precipitation, plane-polarized light. (B) The same field of panel A under cross-polarized light. (C) Biogenic silica precipitated in *Tasmanites* cysts, plane-polarized light; (D) Panel C as seen in cross-polarized light; (E) SEM image (backscattered electron image) of biogenic silica precipitated in *Tasmanites* cysts; (F) SEM image (backscattered electron image) of microcrystalline quartz precipitated in *Tasmanites* cysts and in the matrix. R = radiolaria; T = *Tasmanites* cyst; Qtz = quartz.

of the Blocher Member based on C-S-Fe relationships and redox-sensitive trace element ratios.

5.4. Organic maceral variation

Organic macerals follow specific evolutional pathways during thermal maturation (Peters and Cassa, 1994; Liu et al., 2019). Alginite derived from *Tasmanites* cysts has higher hydrocarbon generation potential (Revill et al., 1994; Vigran et al., 2008), but is more resistant to thermal degradation compared to AOM (Vigran et al., 2008; Liu et al., 2019). The stratigraphic distribution of organic macerals can result in stratigraphic variability of the hydrocarbon generation potential of source rocks (Bohacs, 1993; Chandra et al., 1993; Slatt et al., 2012; Ade and Trindade, 2017). For example, Slatt et al. (2012) reported that cyclic variations of hydrocarbon generation potential in the Barnett Shale resulted from fluctuations of relative sea level at the parasequence scale. Ade and Trindade (2017) reported higher hydrogen index in the TST than in the HST in the southeastern Paraná Basin (Brazil).

The stratigraphic distribution of organic macerals within the New Albany Shale indicates that sea-level fluctuations control selective preservation of organic macerals by influencing bottom-water redox conditions and clastic supply. In the LST, organic macerals are dominated by alginite (Fig. 10). Relative sea level is low and bottom water is oxygenated in the LST, and under such conditions OM undergoes severe

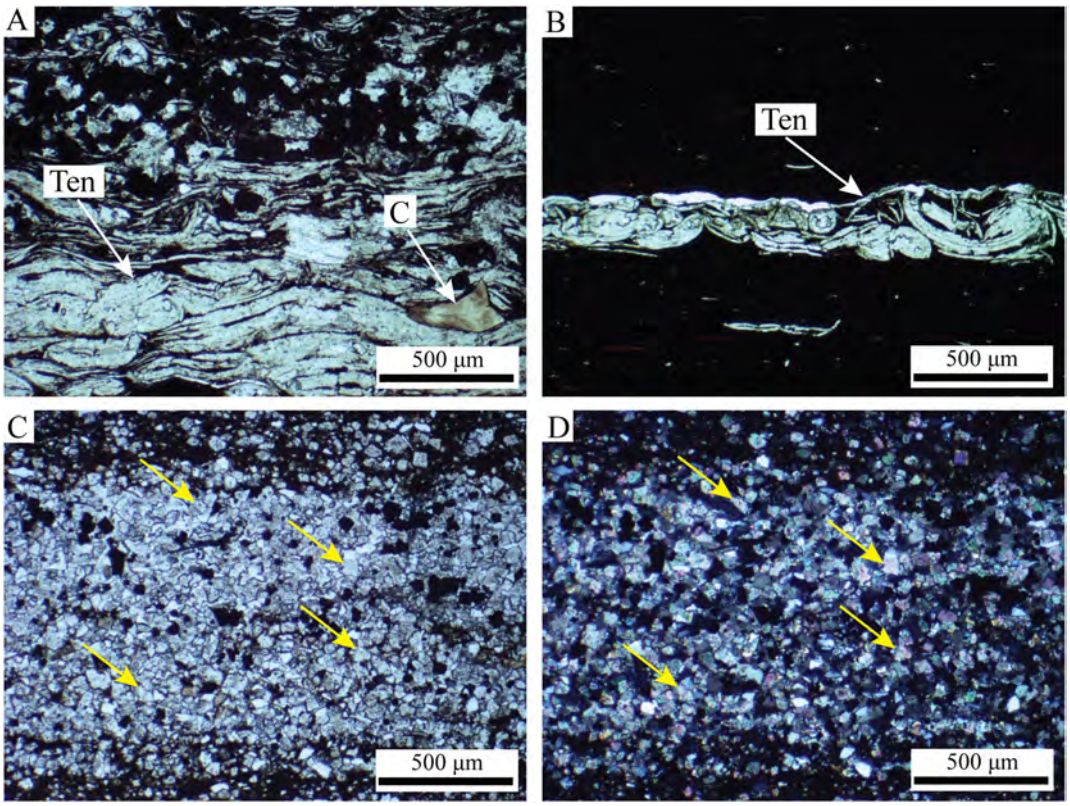

Fig. 14. Photomicrographs of laminae composed of calcareous fossil fragments and recycled dolomite in the Blocher Member. (A–B) Laminae composed *Tentaculites* in the Blocher Member, plane-polarized light; (C) Silty lamina mainly composed of recycled dolomite (yellow arrows), plane-polarized light; (D) The same field of panel C under cross-polarized light. Ten = *Tentaculites*; C = conodont.

microbial breakdown. Labile OM, which will turn into AOM later in diagenesis, would be largely destroyed and relatively resistant algal cysts which will turn into alginite during diagenesis will be enriched. Schieber (2001) also reported that alginite was more abundant than bituminite (a synonym of AOM; Kus et al., 2017) at the base of black shale packages within a given depositional sequence. At the onset of transgression, sea level rises and oxygen content in the bottom water decreases. Labile OM will be better preserved because of reduced microbial degradation. There is a slight decrease of AOM content at the MFS (Fig. 10), probably because sedimentation rates were so low that labile OM stayed on the sea floor long enough to be partially destroyed. The U/Th and Mo/Al ratio profiles also suggest that the most oxygen-deficient conditions did not occur at MFSs (Fig. 6). Schieber (2001) also found that alginite derived from *Tasmanites* cysts was enriched at MFSs in the Chattanooga and New Albany Shale of the eastern USA. As sea level drops, oxygen content in bottom water increases and microbial breakdown of labile OM intensifies. Better oxygenation of bottom waters is indicated by gray bioturbated beds in HSTs (Figs. 2, 3). In the Selmier Member, bioturbation is common and intense (Figs. 2, 3) and OM is dominated by alginite (Fig. 10), suggesting that relatively oxic conditions are not favorable for AOM preservation. In sequence 3, however, the AOM content reaches a maximum in the middle of the HST (Fig. 10). A potential explanation for this could be that increasing clastic supply in the HST improved preservation of AOM because timely cover by clastic materials prevented AOM from microbial breakdown. This is further supported by the coincidence of AOM and Al content maximum at about 625.0 m (Figs. 6, 10). Organic petrographic study of more closely spaced samples is needed to understand the stratigraphic variation of different types of OM and infer the control of depositional conditions on the differential preservation of organic macerals.

Authigenic precipitates of quartz and pyrite in *Tasmanites* cysts have been reported from Devonian black shales of the eastern USA (Schieber, 1996; Schieber et al., 2000; Schieber and Baird, 2001) as a consequence of very low sedimentation rates. These cyst fills are common in the TST and HST, and most prominent at the MFS where sedimentation rates were minimal. In the LST, filled *Tasmanites* cysts occur as well, but the fill in this case consists of detrital materials, such as grains of quartz, K-feldspar, recycled dolomite, mica, pyrite, and clay minerals (Fig. 17). Schieber and Lazar (2004) and Lazar (2007) pointed out that these detrital infills as well as an abundance of broken alga cysts (Fig. 17) are best explained as a consequence of sediments reworking by storm-induced bottom currents during lowstands.

5.5. Influence of relative sea-level fluctuations on OM accumulation

In this study, the stratigraphic distribution of TOC and geochemical proxies indicates that bottom-water redox conditions are one of the controlling factors for OM accumulation within a sequence stratigraphic context (Fig. 6). Clastic supply and paleoproductivity exert additional influences via dilution or preservation.

Relative sea-level fluctuations influence paleoproductivity, clastic supply, bottom-water redox conditions, and their combined control on OM accumulation in epicontinental seas (Arthur and Sageman, 2005). OM content has been linked to sequence stratigraphic context in a number of previous studies (Bohacs, 1993; Chandra et al., 1993; Creaney and Passey, 1993; Slatt and Rodriguez, 2012; Ade and Trindade, 2017; Dong et al., 2017; Byun et al., 2018; Harris et al., 2018), and in general terms, OM preferentially accumulates in TSTs because of lower clastic dilution and bottom-water oxygenation. OM is not as easily preserved in HSTs because of increasing clastic dilution and bottom-water oxygenation due to

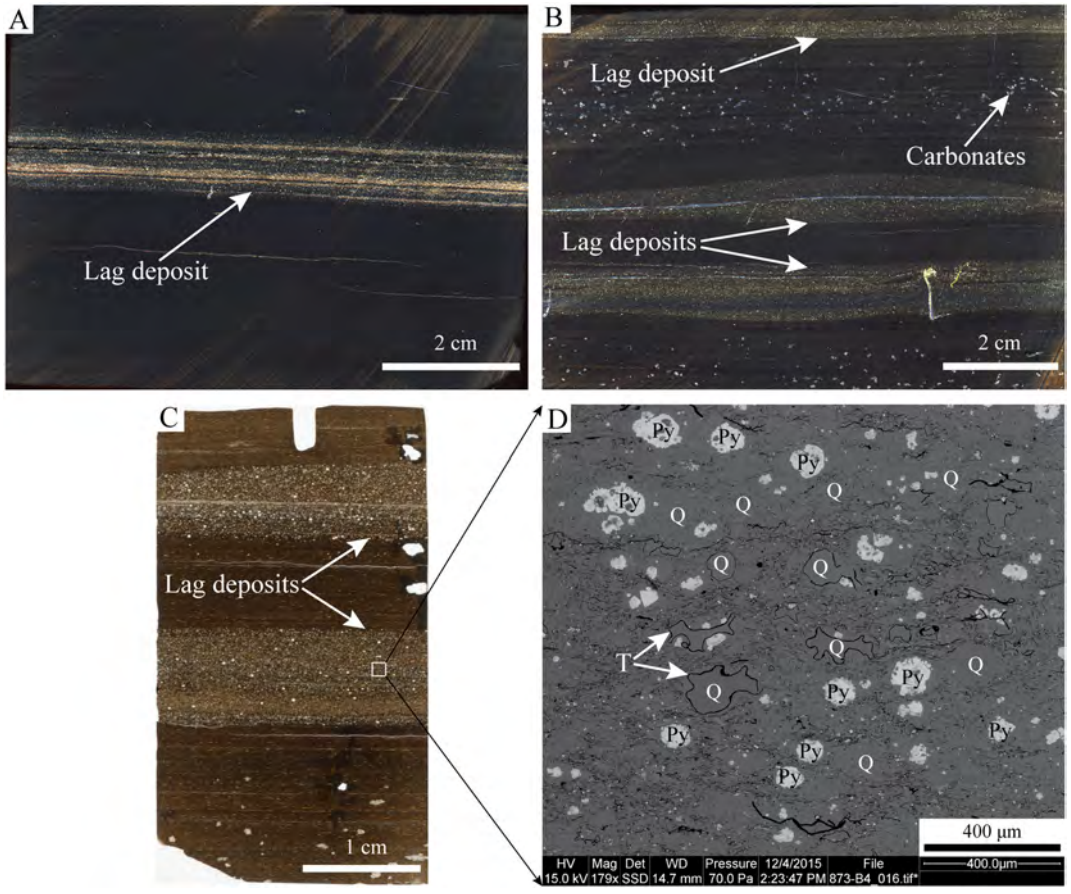

Fig. 15. (A) Scanned core slab showing lag deposits at the MFS of sequence 3 at 632.64 m. (B) Scanned core slab showing lag deposits at the MFS of sequence 4 at 613.85 m. The carbonate nodules suggest low sedimentation rate. (C) Scanned polished thin section of the lower two lags in panel B. (D) SEM image (backscattered electron image) of the rectangular framed area in panel C. Note the *Tasmanites* cysts filled with authigenic quartz. T = *Tasmanites* cyst; Q = quartz; Py = pyrite.

shallowing, and is thought to reach a maximum at the MFS (Creaney and Passey, 1993). As pointed out above, in this study TOC maxima do not coincide with MFSs, presumably because OM residence times were such that substantial amounts of initial OM were remineralized prior to burial. Byun et al. (2018) reported similar TOC distribution patterns in the Middle Ordovician Jigunsan Formation of Korea, but attributed it to the reduction of productivity of benthic biota towards the MFS. The TOC distribution pattern seen in relation to sequence stratigraphic variability in the New Albany Shale may also apply to other black shale successions, which may have different depositional settings and histories. It is noteworthy that the stratigraphic variation of TOC content in black shale successions with high thermal maturity may not represent the variation of OM content when shales were deposited because of petroleum generation and expulsion (Tissot and Welte, 1984) and migration of solid bitumen within black shales (Hackley and Cardott, 2016; Liu et al., 2019).

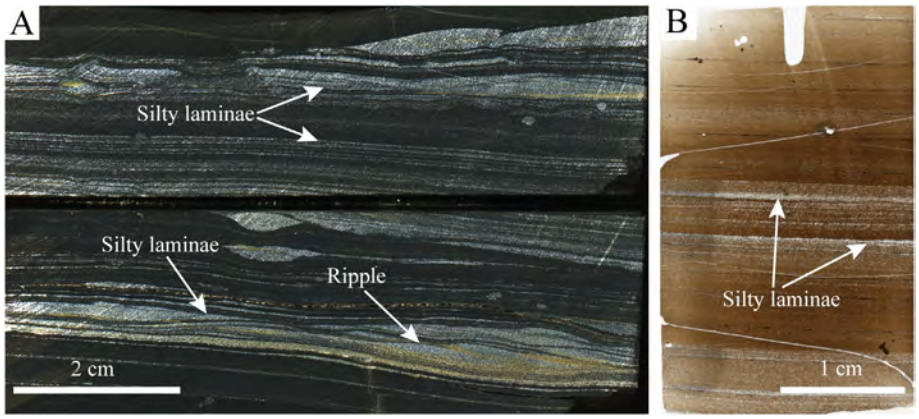

Fig. 16. (A) Scanned core slab showing silty laminae in the Blocher Member. Note the combined-flow ripple in the lower right corner. The laminae are mainly composed of recycled dolomite, quartz, and pyrite. Also note silt-filled burrows and laminae disruptions, an indication of benthic life at the seafloor. (B) Scanned polished thin section of the sample in panel A. Laminae of several grains thick are very common, suggesting frequent storm and wave reworking of bottom sediments.

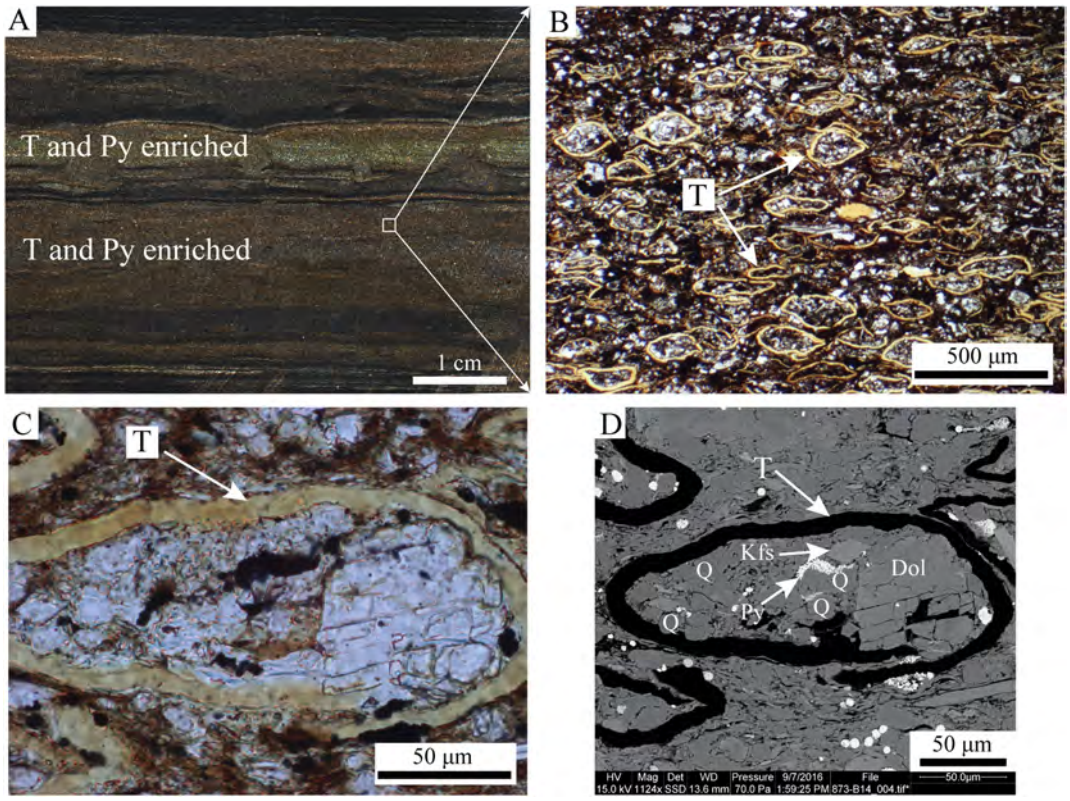

Fig. 17. *Tasmanites* cysts-enriched interval in the LST of sequence 4 at 620.24 m. (A) Scanned core slab showing brownish laminae mainly composed of *Tasmanites* cysts and pyrite. (B) Photomicrograph of the rectangular framed area in panel A, plane-polarized light. *Tasmanites* cysts filled with varying mineral particles. Note that most *Tasmanites* cysts are broken. (C) *Tasmanites* cyst filled with recycled dolomite, quartz, and other mineral particles, plane-polarized light. (D) SEM image (backscattered electron image) of the *Tasmanites* cyst in panel C. The *Tasmanites* cyst is filled with quartz, K-feldspar, recycled dolomite, and pyrite. T = *Tasmanites* cyst; Q = quartz; Dol = dolomite; Kfs = K-feldspar; Py = pyrite.

6. Conclusions

Detailed examination of TOC content, organic petrographic composition, and high-resolution (8 cm spacing) geochemical proxies of the New Albany Shale allow us to evaluate the influence of relative sea-level fluctuations on paleoproductivity, clastic supply, bottom-water redox conditions, and their complex interactions on OM enrichment in marine organic-rich sediments. The key contribution of this study is understanding stratigraphic variation of OM content and type within a sequence stratigraphic context. Specific conclusions can be drawn:

(1) OM content and type in the New Albany Shale vary stratigraphically. The stratigraphic distribution of TOC content and geochemical proxies indicates that bottom-water redox conditions are one of the controlling factors for OM accumulation in the New Albany Shale. Paleoproductivity and clastic supply have dual impacts on OM accumulation; they can enrich or dilute OM.
(2) Relative sea-level fluctuations influence paleoproductivity, clastic supply, bottom-water redox conditions, and their combined control on OM accumulation in the New Albany Shale. Within a sequence stratigraphic context, TOC content increases in TSTs, reaches a maximum before the MFS, and maintains relatively low values during HSTs. The relatively low TOC contents at MFSs reflect a combination of low burial efficiency, elevated bottom-water oxygenation caused by storm reworking, and high levels of dilution by biogenic silica. The stratigraphic variation of organic matter content and type may also apply to other black shale successions and can be beneficial for working out the sequence stratigraphic framework of fine-grained organic-rich sedimentary successions.
(3) OM in the New Albany Shale is dominated by either AOM or alginite (mainly derived from *Tasmanites* cysts). Terrestrial OM (vitrinite + inertinite) content is <10%. AOM content increases in TSTs, reaches a maximum near the MFS, and decreases in HSTs. Increasing clastic supply in HSTs can enhance the preservation of AOM and shift the AOM content maximum to the middle of HSTs. Enrichment of broken and detrital filled *Tasmanites* cysts indicates high-energy environments and LST conditions.
(4) Successful development of oil and gas from tight shale reservoirs requires a good understanding of stratigraphic distribution of TOC and hydrocarbon generation potential because OM plays different roles in shale oil vs shale gas plays (Jarvie, 2012a, 2012b; Bohacs et al., 2013). The results of this study can help better evaluate unconventional petroleum systems.

Supplementary data to this article can be found online at https://doi.org/10.1016/j.sedgeo.2019.02.004.

Acknowledgements

This research was supported by the sponsors of the Indiana University Shale Research Consortium, a Geological Society of America Graduate Student Research Grant, and a Research Grant-in-Aid Award from Department of Earth and Atmospheric Sciences, Indiana University Bloomington. Mastalerz's contribution is based upon work supported by the U.S. Department of Energy, Office of Science, Office of Basic Energy Sciences, Chemical Sciences, Geosciences, and Biosciences Division under Award Number DE-SC0006978. Financial support for B. Liu from the China Scholarship Council is also gratefully acknowledged. We thank Remus Lazar from ExxonMobil Upstream Research Company for sharing his work on and insights into the sequence stratigraphic framework of the New Albany Shale.

References

Abarghani, A., Ostadhassan, M., Gentzis, T., Carvajal-Ortiz, H., Bubach, B., 2018. Organofacies study of the Bakken source rock in North Dakota, USA, based on organic petrology and geochemistry. Int. J. Coal Geol. 188, 79–93.

Adams, J.A.S., Weaver, C.E., 1958. Thorium-to-uranium ratios as indicators of sedimentary processes: example of concept of geochemical facies. AAPG Bull. 42, 387–430.

Ade, M.V.B., Trindade, L.A., 2017. Dispersed organic matter analysis and distribution in the sequence stratigraphic framework of the southeastern, Paraná Basin, Brazil. J. Sediment. Environ. 2, 195–218.

Akar, Ç., Mastalerz, M., Schimmelmann, A., Drobniak, A., 2015. Comparison of hydrocarbon potentials of New Albany Shale and Maquoketa Group in Indiana, USA. Jacobs J. Petrol. Nat. Gas 1, 1–15.

Algeo, T.J., Lyons, T.W., 2006. Mo–total organic carbon covariation in modern anoxic marine environments: Implications for analysis of paleoredox and paleohydrographic conditions. Paleoceanography 21, PA1016. https://doi.org/10.1029/2004PA001112.

Algeo, T.J., Tribovillard, N., 2009. Environmental analysis of paleoceanographic systems based on molybdenum–uranium covariation. Chem. Geol. 268, 211–225.

Algeo, T.J., Kuwahara, K., Sano, H., Bates, S., Lyons, T., Elswick, E., Hinnov, L., Ellwood, B., Moser, J., Maynard, J.B., 2011. Spatial variation in sediment fluxes, redox conditions, and productivity in the Permian–Triassic Panthalassic Ocean. Palaeogeogr. Palaeoclimatol. Palaeoecol. 308, 65–83.

Algeo, T.J., Henderson, C.M., Tong, J., Feng, Q., Yin, H., Tyson, R.V., 2013. Plankton and productivity during the Permian–Triassic boundary crisis: An analysis of organic carbon fluxes. Glob. Planet. Chang. 105, 52–67.

Anderson, R.F., Fleisher, M.Q., LeHuray, A.P., 1989. Concentration, oxidation state, and particulate flux of uranium in the Black Sea. Geochim. Cosmochim. Acta 53, 2215–2224.

Arthur, M.A., Sageman, B.B., 2005. Sea-level control on source-rock development: Perspectives from the Holocene Black Sea, the mid-Cretaceous Western Interior Basin of North America, and the Late Devonian Appalachian Basin. In: Harris, N.B. (Ed.), The Deposition of Organic-Carbon Rich Sediments: Models, Mechanisms, and Consequences. SEPM Special Publication 82, pp. 35–59.

Beier, J.A., Hayes, J.M., 1989. Geochemical and isotopic evidence for paleoredox conditions during deposition of the Devonian-Mississippian New Albany Shale, southern Indiana. Geol. Soc. Am. Bull. 101, 774–782.

Bialkowski, A., Tribovillard, N., Vergès, E., Deconinck, J.-F., 2000. Sedimentary organic matter, accumulation and grain-size in the Kimmeridgian–Tithonian of the Boulonnais area (Northern France). Application to sequence stratigraphy. C. R. Acad. Sci. Ser. IIA Earth Planet. Sci. 331, 451–458.

Bohacs, K.M., 1993. Source quality variations tied to sequence development in the Monterey and associated formations, southwestern California. In: Katz, B.J., Pratt, L.M. (Eds.), Source Rocks in a Sequence Stratigraphic Framework. AAPG Studies in Geology 37, pp. 177–204.

Bohacs, K.M., Schwalbach, J.R., 1994. Natural gamma-ray spectrometry of the Monterey Formation at Naples Beach, California: insights into lithology, stratigraphy, and source-rock quality. In: Hornafius, J.S. (Ed.), Field Guide to the Monterey Formation between Santa Barbara and Gaviota, California. AAPG Pacific Section GB 72, pp. 85–94.

Bohacs, K.M., Grabowski Jr., G.J., Carroll, A.R., Mankiewicz, P.J., Miskell-Gerhardt, K.J., Schwalbach, J.R., Wegner, M.B., Simo, J.A., 2005. Production, destruction, and dilution—the many paths to source-rock development. In: Harris, N.B. (Ed.), The Deposition of Organic-Carbon Rich Sediments: Models, Mechanisms, and Consequences. SEPM Special Publication 82, pp. 61–101.

Bohacs, K.M., Passey, Q.R., Rudnicki, M., Esch, W.L., Lazar, O.R., 2013. The spectrum of fine-grained reservoirs from 'shale gas' to 'shale oil'/tight liquids: essential attributes, key controls, practical characterization. International Petroleum Technology Conference. Beijing, China, March 26–28, 2013, Paper IPTC 16676 https://doi.org/10.2523/IPTC-16676-MS.

Bralower, T.J., Thierstein, H.R., 1987. Organic carbon and metal accumulation rates in Holocene and mid-Cretaceous sediments: palaeoceanographic significance. Geol. Soc. Lond., Spec. Publ. 26, 345–369.

Brett, C.E., Baird, G.C., Bartholomew, A.J., 2004. Sequence stratigraphy of highly variable Middle Devonian strata in central Kentucky: Implications for regional correlations and depositional environments. In: Schieber, J., Lazar, R.O. (Eds.), Devonian Black Shales of the Eastern U.S.: New Insights into Sedimentology and Stratigraphy from the Subsurface and Outcrops in the Illinois and Appalachian Basins. Field Guide for the 2004 Annual Field Conference of the Great Lakes Section of SEPM, Indiana Geological Survey Open File Study, 04–05, pp. 35–60.

Brumsack, H.J., 2006. The trace metal content of recent organic carbon-rich sediments: implications for Cretaceous black shale formation. Palaeogeogr. Palaeoclimatol. Palaeoecol. 232, 344–361.

Byun, U.H., Lee, H.S., Kwon, Y.K., 2018. Sequence stratigraphy in the middle Ordovician shale successions, mid-east Korea: stratigraphic variations and preservation potential of organic matter within a sequence stratigraphic framework. J. Asian Earth Sci. 152, 116–131.

Calvert, S.E., Pedersen, T.F., 1993. Geochemistry of recent oxic and anoxic marine sediments: Implications for the geological record. Mar. Geol. 113, 67–88.

Calvert, S.E., Bustin, R.M., Ingall, E.D., 1996. Influence of water column anoxia and sediment supply on the burial and preservation of organic carbon in marine shales. Geochim. Cosmochim. Acta 60, 1577–1593. https://doi.org/10.1016/0016-7037(96)00041-5.

Campbell, G., 1946. New Albany Shale. GSA Bull. 57, 829–908.

Chandra, K., Raju, D.S.N., Mishra, P.K., 1993. Sea level changes, anoxic conditions, organic matter enrichment, and petroleum source rock potential of the Cretaceous sequences of the Cauvery Basin, India. In: Katz, B.J., Pratt, L.M. (Eds.), Source Rocks in a Sequence Stratigraphic Framework. AAPG Studies in Geology 37, pp. 131–146.

Chou, M.-I.M., Dickerson, D.R., Chou, S.-F.J., Sargent, M.L., 1991. Hydrocarbon Source Potential and Organic Geochemical Nature of Source Rocks and Crude Oils in the Illinois Basin. 136. Illinois State Geological Survey, Champaign, Illinois, USA (39 pp).

Creaney, S., Passey, Q.R., 1993. Recurring patterns of total organic carbon and source rock quality within a sequence stratigraphic framework. AAPG Bull. 77, 386–401.

Cumberland, S.A., Douglas, G., Grice, K., Moreau, J.W., 2016. Uranium mobility in organic matter-rich sediments: A review of geological and geochemical processes. Earth Sci. Rev. 159, 160–185.

Curtis, C.D., 1980. Diagenetic alteration in black shales. J. Geol. Soc. 137, 189–194.

Dickinson, W.R., Beard, L.S., Brakenridge, G.R., Erjavec, J.L., Ferguson, R.C., Inman, K.F., Knepp, R.A., Lindberg, F.A., Ryberg, P.T., 1983. Provenance of North American Phanerozoic sandstones in relation to tectonic setting. GSA Bull. 94, 222–235.

Dong, T., Harris, N.B., Ayranci, K., 2017. Relative sea-level cycles and organic matter accumulation in shales of the Middle and Upper Devonian Horn River Group, northeastern British Columbia, Canada: Insights into sediment flux, redox conditions, and bioproductivity. GSA Bull. 130, 859–880.

Ettensohn, F.R., 2008. The Appalachian foreland basin in eastern United States. In: Miall, A.D. (Ed.), The Sedimentary Basins of the United States and Canada. Elsevier, Amsterdam, pp. 105–179.

Fertl, W.H., Chilingar, G.V., 1988. Total organic carbon content determined from well logs. SPE Form. Eval. 3, 407–419.

Goñi, M.A., Ruttenberg, K.C., Eglinton, T.I., 1997. Sources and contribution of terrigenous organic carbon to surface sediments in the Gulf of Mexico. Nature 389, 275–278.

Gregory, W.A., Hart, G.F., 1992. Towards a predictive model for the palynologic response to sea-level changes. Palaios 7, 3–33.

Hackley, P.C., Cardott, B.J., 2016. Application of organic petrography in North American shale petroleum systems: A review. Int. J. Coal Geol. 163, 8–51.

Hamilton-Smith, T., Hasenmueller, N.R., Boberg, W.S., Smidchens, Z., Frankie, W.T., 1994. Gas production. In: Hasenmueller, N.R., Comer, J.B. (Eds.), Gas Potential of the New Albany Shale (Devonian and Mississippian) in the Illinois Basin. Gas Research Institute, GRI-00/0068, Illinois Basin Studies 2, pp. 23–40.

Harris, N.B., McMillan, J.M., Knapp, L.J., Mastalerz, M., 2018. Organic matter accumulation in the Upper Devonian Duvernay Formation, Western Canada Sedimentary Basin, from sequence stratigraphic analysis and geochemical proxies. Sediment. Geol. 376, 185–203.

Hatch, J.R., Leventhal, J.S., 1992. Relationship between inferred redox potential of the depositional environment and geochemistry of the Upper Pennsylvanian (Missourian) Stark Shale Member of the Dennis Limestone, Wabaunsee County, Kansas, USA. Chem. Geol. 99, 65–82.

Hedges, J.I., Keil, R.G., Benner, R., 1997. What happens to terrestrial organic matter in the ocean? Org. Geochem. 27, 195–212.

Ingall, E.D., Bustin, R.M., Van Cappellen, P., 1993. Influence of water column anoxia on the burial and preservation of carbon and phosphorus in marine shales. Geochim. Cosmochim. Acta 57, 303–316.

Jacob, H., 1989. Classification, structure, genesis and practical importance of natural solid oil bitumen ("migrabitumen"). Int. J. Coal Geol. 11, 65–79.

Jarvie, D.M., 2012a. Shale resource systems for oil and gas: Part 1—shale-gas resource systems. In: Breyer, J.A. (Ed.), Shale Reservoirs— Giant Resources for the 21st Century. AAPG Memoir 97, pp. 69–87.

Jarvie, D.M., 2012b. Shale resource systems for oil and gas: Part 2—shale-oil resource systems. In: Breyer, J.A. (Ed.), Shale Reservoirs—Giant Resources for the 21st Century. AAPG Memoir 97, pp. 89–119.

Jones, B., Manning, D.A., 1994. Comparison of geochemical indices used for the interpretation of palaeoredox conditions in ancient mudstones. Chem. Geol. 111, 111–1129.

Killops, S., Killops, V., 2005. Introduction to Organic Geochemistry. second ed. Blackwell Publishing, Malden, MA, USA (406 pp.).

Klinkhammer, G.P., Palmer, M.R., 1991. Uranium in the oceans: where it goes and why. Geochim. Cosmochim. Acta 55, 1799–1806.

Kus, J., Araujo, C.V., Borrego, A.G., Flores, D., Hackley, P.C., Hámor-Vidó, M., Kalaitzidis, S., Kommeren, C.J., Kwiecińska, B., Mastalerz, M., Mendonça Filho, J.G., Menezes, T.R., Misz-Kennan, M., Nowak, G.J., Petersen, H.I., Rallakis, D., Suárez-Ruiz, I., Sýkorová, I., Životič, D., 2017. Identification of alginite and bituminite in rocks other than coal. 2006, 2009, and 2011 round robin exercises of the ICCP Identification of Dispersed Organic Matter Working Group. Int. J. Coal Geol. 178, 26–38.

Langmuir, D., 1978. Uranium solution-mineral equilibria at low temperatures with applications to sedimentary ore deposits. Geochim. Cosmochim. Acta 42, 547–569.

Lash, G., Blood, R., 2011. Sequence stratigraphy as expressed by shale source rock and reservoir characteristics—Examples from the Devonian succession, Appalachian Basin. AAPG Annual Convention and Exhibition, Houston, TX, USA, April 10-13, 2011, 80168.

Lazar, O.R., 2007. Redefinition of the New Albany Shale of the Illinois Basin: An Integrated, Stratigraphic, Sedimentologic, and Geochemical Study. (Ph.D. dissertation). Indiana University, Bloomington (336 pp.). https://search.proquest.com/docview/304849382?pq-origsite=gscholar.

Leventhal, J.S., 1981. Pyrolysis gas chromatography-mass spectrometry to characterize organic matter and its relationship to uranium content of Appalachian Devonian black shales. Geochim. Cosmochim. Acta 45, 883–889.

Lewan, M.D., Maynard, J.B., 1982. Factors controlling enrichment of vanadium and nickel in the bitumen of organic sedimentary rocks. Geochim. Cosmochim. Acta 46, 2547–2560.

Lineback, J.A., 1964. Stratigraphy and Depositional Environment of the New Albany Shale (Upper Devonian and Lower Mississippian) in Indiana. (Ph.D. dissertation). Indiana University (136 pp.).

Lineback, J.A., 1968. Subdivisions and depositional environments of New Albany Shale (Devonian-Mississippian) in Indiana. AAPG Bull. 52, 1291–1303.

Liu, B., Schieber, J., Mastalerz, M., 2017. Combined SEM and reflected light petrography of organic matter in the New Albany Shale (Devonian-Mississippian) in the Illinois Basin: A perspective on organic pore development with thermal maturation. Int. J. Coal Geol. 184, 57–72.
Liu, B., Schieber, J., Mastalerz, M., 2019. Petrographic and micro-FTIR study of organic matter in the Upper Devonian New Albany Shale During thermal maturation: Implications for kerogen transformation. https://doi.org/10.1306/13672216M1213380.
Loucks, R.G., Reed, R.M., Ruppel, S.C., Hammes, U., 2012. Spectrum of pore types and networks in mudrocks and a descriptive classification for matrix-related mudrock pores. AAPG Bull. 96, 1071–1098.
Lüning, S., Kolonic, S., 2003. Uranium spectral gamma-ray response as a proxy for organic richness in black shales: applicability and limitations. J. Pet. Geol. 26, 153–174.
Mastalerz, M., Schimmelmann, A., Lis, G.P., Drobniak, A., Stankiewicz, A., 2012. Influence of maceral composition on geochemical characteristics of immature shale kerogen: insight from density fraction analysis. Int. J. Coal Geol. 103, 60–69.
Mastalerz, M., Schimmelmann, A., Drobniak, A., Chen, Y., 2013. Porosity of Devonian and Mississippian New Albany Shale across a maturation gradient: insights from organic petrology, gas adsorption, and mercury intrusion. AAPG Bull. 97, 1621–1643.
Mastalerz, M., Drobniak, A., Stankiewicz, A.B., 2018. Origin, properties, and implications of solid bitumen in source-rock reservoirs: A review. Int. J. Coal Geol. 195, 14–36.
McLaughlin, P.I., Emsbo, P., Desrochers, A., Bancroft, A., Brett, C.E., Riva, J.F., Premo, W., Neymark, L., Achab, A., Asselin, E., Emmons, M.M., 2016. Refining 2 km of Ordovician chronostratigraphy beneath Anticosti Island utilizing integrated chemostratigraphy. Can. J. Earth Sci. 53, 865–874.
Morford, J.L., Emerson, S., 1999. The geochemistry of redox sensitive trace metals in sediments. Geochim. Cosmochim. Acta 63, 1735–1750.
Müller, P.J., Suess, E., 1979. Productivity, sedimentation rate, and sedimentary organic matter in the oceans—I. Organic carbon preservation. Deep Sea Res. A Oceanogr. Res. Pap. 26, 1347–1362.
Nuttall, B.C., Parris, T.M., Beck, G., Willette, D.C., Mastalerz, M., Crockett, J., 2015. Oil Production from Low-maturity Organic-rich Shale: an example from the Devonian New Albany Shale in the Illinois Basin, Breckinridge County, Kentucky. AAPG Eastern Section 44th Annual Meeting, Indianapolis, Indiana, September 20-22, 2015, 51196.
Ocubalidet, S.G., Rimmer, S.M., Conder, J.A., 2018. Redox conditions associated with organic carbon accumulation in the Late Devonian New Albany Shale, west-central Kentucky, Illinois Basin. Int. J. Coal Geol. 190, 42–55.
Opsahl, S., Benner, R., 1997. Distribution and cycling of terrigenous dissolved organic matter in the ocean. Nature 386, 480–482.
Pacton, M., Gorin, G.E., Vasconcelos, C., 2011. Amorphous organic matter—experimental data on formation and the role of microbes. Rev. Palaeobot. Palynol. 166, 253–267.
Pasley, M.A., Gregory, W.A., Hart, G.F., 1991. Organic matter variations in transgressive and regressive shales. Org. Geochem. 17, 483–509.
Passey, Q.R., Bohacs, K.M., Esch, W.L., Klimentidis, R., Sinha, S., 2010. From oil-prone source rock to gas-producing shale reservoir-geologic and petrophysical characterization of unconventional shale-gas reservoirs. Chinese Petroleum Society/Society of Petroleum Engineers International Oil and Gas Conference and Exhibition, Beijing, China, June 8–10, 2010, SPE Paper 131350 https://doi.org/10.2118/131350-MS.
Pedersen, T.F., Calvert, S.E., 1990. Anoxia vs. productivity: what controls the formation of organic-carbon-rich sediments and sedimentary Rocks? AAPG Bull. 74, 454–466.
Peters, K.E., Cassa, M.R., 1994. Applied source rock geochemistry. In: Magoon, L.B., Dow, W.G. (Eds.), The Petroleum System—From Source to Trap. AAPG Memoir vol. 60, pp. 93–120.
Ponsaing, L., Bojesen-Koefoed, J.A., Thomsen, E., Stemmerik, L., 2018. Temporal organic facies variations of Upper Jurassic-lowermost Cretaceous source rocks in the Danish Central Graben, North Sea. Int. J. Coal Geol. 195, 217–237.
Raiswell, R., Berner, R.A., 1987. Organic carbon losses during burial and thermal maturation of normal marine shales. Geology 15, 853–856.
Revill, A.T., Volkman, J.K., O'leary, T., Summons, R.E., Boreham, C.J., Banks, M.R., Denwer, K., 1994. Hydrocarbon biomarkers, thermal maturity, and depositional setting of tasmanite oil shales from Tasmania, Australia. Geochim. Cosmochim. Acta 58, 3803–3822.
Rimmer, S.M., 2004. Geochemical paleoredox indicators in Devonian–Mississippian black shales, central Appalachian Basin (USA). Chem. Geol. 206, 373–391.
Rimmer, S.M., Thompson, J.A., Goodnight, S.A., Robl, T.L., 2004. Multiple controls on the preservation of organic matter in Devonian–Mississippian marine black shales: geochemical and petrographic evidence. Palaeogeogr. Palaeoclimatol. Palaeoecol. 215, 125–154.
Ripley, E.M., Shaffer, N.R., Gilstrap, M.S., 1990. Distribution and geochemical characteristics of metal enrichment in the New Albany Shale (Devonian-Mississippian), Indiana. Econ. Geol. 85, 1790–1807.
Robison, V.D., Liro, L.M., Robison, C.R., Dawson, W.C., Russo, J.W., 1996. Integrated geochemistry, organic petrology, and sequence stratigraphy of the Triassic Shublik Formation, Tenneco Phoenix # 1 well, North Slope, Alaska, USA. Org. Geochem. 24, 257–272.
Robl, T.L., Rimmer, S.M., Barron, L.S., 1992. Organic petrography of Mississippian and Devonian shales in east-central Kentucky. Fuel 71, 267–271.
Ross, D.J.K., Bustin, R.M., 2009. The importance of shale composition and pore structure upon gas storage potential of shale gas reservoirs. Mar. Pet. Geol. 26, 916–927.
Rowe, H., Hughes, N., Robinson, K., 2012. The quantification and application of handheld energy-dispersive X-ray fluorescence (ED-XRF) in mudrock chemostratigraphy and geochemistry. Chem. Geol. 324, 122–131.
Sageman, B.B., Murphy, A.E., Werne, J.P., Ver Straeten, C.A., Hollander, D.J., Lyons, T.W., 2003. A tale of shales: the relative roles of production, decomposition, and dilution in the accumulation of organic-rich strata, Middle–Upper Devonian, Appalachian basin. Chem. Geol. 195, 229–273.
Schenau, S.J., Reichart, G.J., De Lange, G.J., 2005. Phosphorus burial as a function of paleoproductivity and redox conditions in Arabian Sea sediments. Geochim. Cosmochim. Acta 69, 919–931.
Schieber, J., 1996. Early diagenetic silica deposition in algal cysts and spores: a source of sand in black shales? J. Sediment. Res. 66, 175–183.
Schieber, J., 1998. Developing a sequence stratigraphic framework for the Late Devonian Chattanooga Shale of the southeastern USA: relevance for the Bakken Shale. In: Christopher, J.E., Gilboy, C.F., Paterson, D.F., Bend, S.L. (Eds.), Eighth International Williston Basin Symposium. Saskatchewan Geological Society Special Publication 13, pp. 58–68.
Schieber, J., 2001. A role for organic petrology in integrated studies of mudrocks: examples from Devonian black shales of the eastern US. Int. J. Coal Geol. 47, 171–187.
Schieber, J., 2009. Discovery of agglutinated benthic foraminifera in Devonian black shales and their relevance for the redox state of ancient seas. Palaeogeogr. Palaeoclimatol. Palaeoecol. 271, 292–300.
Schieber, J., 2010. Common themes in the formation and preservation of intrinsic porosity in shales and mudstones-illustrated with examples across the Phanerozoic. SPE Unconventional Gas Conference. Society of Petroleum Engineers, Pittsburgh, Pennsylvania, USA. SPE 132370 https://doi.org/10.2118/132370-MS.
Schieber, J., 2016. Mud re-distribution in epicontinental basins–Exploring likely processes. Mar. Pet. Geol. 71, 119–133.
Schieber, J., Baird, G., 2001. On the origin and significance of pyrite spheres in Devonian black shales of North America. J. Sediment. Res. 71, 155–166.
Schieber, J., Lazar, R.O., 2004. Devonian Black Shales of the Eastern U.S.: New Insights into Sedimentology and Stratigraphy from the Subsurface and Outcrops in the Illinois and Appalachian Basins. Indiana Geological Survey Open File Study 04–05 (90 pp.).
Schieber, J., Krinsley, D., Riciputi, L., 2000. Diagenetic origin of quartz silt in mudstones and implications for silica cycling. Nature 406, 981–985.
Schoepfer, S.D., Shen, J., Wei, H., Tyson, R.V., Ingall, E., Algeo, T.J., 2015. Total organic carbon, organic phosphorus, and biogenic barium fluxes as proxies for paleomarine productivity. Earth Sci. Rev. 149, 23–52.
Schwalbach, J.R., Bohacs, K.M., 1992. Sequence Stratigraphy in Fine-grained Rocks: Examples from the Monterey Formation. Pacific Section SEPM 70 (80 pp.).
Shaw, T.J., Sholkovitz, E.R., Klinkhammer, G., 1994. Redox dynamics in the Chesapeake Bay: the effect on sediment/water uranium exchange. Geochim. Cosmochim. Acta 58, 2985–2995.
Slatt, R.M., Rodriguez, N.D., 2012. Comparative sequence stratigraphy and organic geochemistry of gas shales: commonality or coincidence? J. Nat. Gas Sci. Eng. 8, 68–84.
Slatt, R.M., Philp, P.R., Abousleiman, Y., Singh, P., Perez, R., Portas, R., Marfurt, K.J., Madrid-Arroyo, S., O'Brien, N., Eslinger, E., Baruch, E.T., 2012. Pore-to-regional-scale integrated characterization workflow for unconventional gas shales. In: Breyer, J.A. (Ed.), Shale Reservoirs — Giant Resources for the 21st Century. AAPG Memoir vol. 97, pp. 127–150.
Spencer, S., 2013. A Sedimentologic, Petrographic, Mineralogic, and Geochemical Investigation of Parasequences in the Camp Run Member of the Late Devonian New Albany Shale. (Master Thesis). Indiana University, Bloomington (338 pp.).
Stach, E., Mackowsky, M.-T.H., Teichmüller, M., Taylor, G.H., Chandra, D., Teichmüller, R., 1982. Stach's Textbook of Coal Petrology. third ed. Gebrüder Borntraeger, Berlin-Stuttgart (535 pp.).
Stasiuk, L.D., Fowler, M.G., 2004. Organic facies in Devonian and Mississippian strata of Western Canada Sedimentary Basin: relation to kerogen type, paleoenvironment, and paleogeography. Bull. Can. Petrol. Geol. 52, 234–255.
Strąpoć, D., Mastalerz, M., Schimmelmann, A., Drobniak, A., Hasenmueller, N.R., 2010. Geochemical constraints on the origin and volume of gas in the New Albany Shale (Devonian–Mississippian), eastern Illinois Basin. AAPG Bull. 94, 1713–1740.
Swanson, V.E., 1960. Oil yield and uranium content of black shales. USGS Professional Paper 356-A (44 pp.).
Tappan, H., 1980. The Paleobiology of Plant Protists. Freeman, San Francisco (1028 pp.).
Taylor, S.R., McLennan, S.M., 1985. The Continental Crust: Its Composition and Evolution. Blackwell, Oxford, pp. 24–29.
Taylor, G.H., Teichmüller, M., Davis, A., Diessel, C.F.K., Littke, R., Robert, P., 1998. Organic Petrology. Gebrüder Borntraeger, Berlin-Stuttgart (704 pp.).
Teichmüller, M., 1989. The genesis of coal from the viewpoint of coal petrology. Int. J. Coal Geol. 12, 1–87.
Tissot, B.P., Welte, D.H., 1984. Petroleum Formation and Occurrence. 2nd ed. Springer-Verlag, Berlin (699 pp.).
Tissot, B., Durand, B., Espitalié, J., Combaz, A., 1974. Influence of nature and diagenesis of organic matter in formation of petroleum. AAPG Bull. 58, 499–506.
Tribovillard, N., Algeo, T.J., Lyons, T., Riboulleau, A., 2006. Trace metals as paleoredox and paleoproductivity proxies: An update. Chem. Geol. 232, 12–32.
Tribovillard, N., Algeo, T.J., Baudin, F., Riboulleau, A., 2012. Analysis of marine environmental conditions based onmolybdenum–uranium covariation—Applications to Mesozoic paleoceanography. Chem. Geol. 324, 46–58.
Tyson, R.V., 1995. Sedimentary Organic Matter: Organic Facies and Palynofacies. Chapman & Hall, London (615 pp.).
Tyson, R.V., Pearson, T.H., 1991. Modern and ancient continental shelf anoxia: an overview. In: Tyson, R.V., Pearson, T.H. (Eds.), Modern and Ancient Continental Shelf Anoxia. Geological Society, London, Special Publication 58, pp. 1–26.
Vigran, J.O., Mørk, A., Forsberg, A.W., Weiss, H.M., Weitschat, W., 2008. *Tasmanites* algae—contributors to the Middle Triassic hydrocarbon source rocks of Svalbard and the Barents Shelf. Polar Res. 27, 360–371.

Wang, F.P., Reed, R.M., John, A., Katherine, J., 2009. Pore networks and fluid flow in gas shales. SPE Annual Technical Conference and Exhibition. Society of Petroleum Engineers, New Orleans, Louisiana, USA. SPE 124253 https://doi.org/10.2118/124253-MS.
Wedepohl, K.H., 1971. Environmental influences on the chemical composition of shales and clays. Phys. Chem. Earth 8, 307–333.
Wei, L., Wang, Y., Mastalerz, M., 2016. Comparative optical properties of macerals and statistical evaluation of mis-identification of vitrinite and solid bitumen from early mature Middle Devonian–Lower Mississippian New Albany Shale: Implications for thermal maturity assessment. Int. J. Coal Geol. 168, 222–236.
Wignall, P.B., 1991. Model for transgressive black shales? Geology 19, 167–170.
Zhao, J., Jin, Z., Jin, Z., Wen, X., Geng, Y., 2017. Origin of authigenic quartz in organic-rich shales of the Wufeng and Longmaxi Formations in the Sichuan Basin, South China: implications for pore evolution. J. Nat. Gas Sci. Eng. 38, 21–38.